Femtosecond real-time probing of reactions. VIII. The bimolecular reaction $Br+I_2$

I. R. Sims,[a] M. Gruebele,[b] E. D. Potter, and A. H. Zewail
Arthur Amos Noyes Laboratory of Chemical Physics, California Institute of Technology, Pasadena, California 91125

(Received 13 February 1992; accepted 8 June 1992)

In this paper, we discuss the experimental technique for real-time measurement of the lifetimes of the collision complex of bimolecular reactions. An application to the atom–molecule $Br+I_2$ reaction at two collision energies is made. Building on our earlier Communication [J. Chem. Phys. **95**, 7763 (1991)], we report on the observed transients and lifetimes for the collision complex, the nature of the transition state, and the dynamics near threshold. Classical trajectory calculations provide a framework for deriving the global nature of the reactive potential energy surface, and for discussing the real-time, scattering, and asymptotic (product-state distribution) aspects of the dynamics. These experimental and theoretical results are compared with the extensive array of kinetic, crossed beam, and theoretical studies found in the literature for halogen radical–halogen molecule exchange reactions.

I. INTRODUCTION

In real-time studies of reaction dynamics, attention has been focused upon different types of unimolecular reactions, either on the femtosecond (fs) time scale, or on the picosecond (ps) time scale for reactions governed by energy redistribution.[1] The first example of a bimolecular reaction studied in real time is $H+CO_2\rightarrow OH+CO$ within an $HI\cdot CO_2$ van der Waals complex.[2] In a recent Communication,[3] we have reported on studies of a different class of bimolecular reactions, atom– (or radical–) molecule, with two objectives: (1) to extend the ps studies[2] to the femtosecond regime; and (2) to clock the bimolecular encounter under unperturbed and isolated conditions on the ground state potential energy surface (PES).

The femtosecond extension was achieved by building a new fs/molecular beam system, which we describe in detail here. The study of isolated bimolecular reactions was initiated in halogen exchange reactions. By making the heavier atom or radical in the dissociated precursor the reactive partner, the lighter fragment rapidly departs from the scene and leaves the bimolecular reaction to occur unperturbed by the presence of a third body. The elementary reaction of interest for this study is

$$Br+I_2\rightarrow [BrI_2]^{\ddagger}\rightarrow BrI+I.$$

The zero of time is defined within the $HBr\cdot I_2$ van der Waals complex, and the light hydrogen atom is some 20 Å away from the field of the reaction in $\approx$100 fs. A fuller account of the earlier Communication[3] is given here.

The paper is outlined as follows. We begin with a discussion of the problem of establishing the zero of time in studies of bimolecular reactions, followed by a discussion of the $Br+I_2$ reaction and related systems, and a discussion of the experimental technique. We then describe in some detail the experimental procedure. The results are analyzed and discussed with focus on bonding in the collision complex and on the dynamics on the reactive surface. Classical trajectory simulations on an optimized PES are used as a guide, and comparison with experiments is made.

II. THE ZERO OF TIME, THE REACTION, AND THE TECHNIQUE

A. Establishing the zero of time

The problem of establishing the zero of time for a bimolecular reaction is different from that in unimolecular reactions. In the unimolecular case, a fs pump laser pulse initiates the simultaneous dissociation of a large number of molecules which all pass essentially together through the transition state region and out to products. A second fs probe pulse can thus interact with a considerable concentration of transient species at any time during the reaction, as illustrated in the studies of many reactions.[1]

Bimolecular radical–molecule reactions are usually investigated by flowing a mixture of a molecular partner and a radical precursor in a cell and photolyzing the precursor to generate radicals which then proceed to react after colliding with the molecular species. The progress of the reaction is then usually monitored by LIF (laser-induced fluorescence) of either the radical species or a reaction product. This method will not work, however, if we wish to probe short-lived intermediates or transition states of the bimolecular reaction, as instead of all the radicals produced by the pump laser pulse proceeding to react with their molecular partners on a fs–ps time scale, a random delay is introduced before collision occurs and the reaction can proceed. This differs for each individual reactive event, lasting typically on the order of 100 ns. Thus the time resolution induced by the ultrafast pump pulse is smeared out over this much longer time period in a random fashion. Furthermore, as a result, the concentration of intermediate

[a]SERC-NATO post-doctoral fellow from UK. Present address: Département de Physique Atomique et Moléculaire, Université de Rennes I, Campur de Beaulieu, 35042 Rennes Cedex, France.
[b]Present address: Department of Chemistry, University of Illinois, Urbana, Illinois 61801.

 0021-9606/92/184127-22$006.00

or transition state species at any one time becomes less for the probe laser to detect. Even in crossed molecular beams, the interaction region (≈ 8 mm^3 for skimmed beams) and beam velocities (typically 100–1000 m/s) result in an "interaction time" in the μs range, making temporal resolution of two reactant beams interacting with a laser beam in this fashion, impossible at the femtosecond level.

However, there are so far two ways of circumventing the problem.[2,4] In the approach by Scherer *et al.*[2] the two initial species, the radical precursor and the reagent molecule, are locked in a van der Waals complex using the elegant methodology (for studies of product state distributions) developed by the groups of Wittig[5] and Soep[6] in what can be called a "precursor geometry limited" (PGL) reaction. To define the zero of time, Scherer *et al.* used an initial ps pulse to photolyze the radical precursor. The newly produced radical partner collides with the molecule after a uniform and short (subpicosecond to picosecond) delay. Subsequent production of reaction intermediates and decay to products can then be observed by a second pulse which is able to interact with a considerable concentration of the transient species. The zero of time is thus defined by the pump pulse with a constant, short delay introduced by the van der Waals bond distance. For this reason, this class of reactions was called van der Waals impacted bimolecular reactions (VIB).[2]

This technique has principally been applied to the reaction $H+CO_2 \rightarrow OH+CO$ within $IH\cdot CO_2$ to study the dynamics of the collision complex $[HOCO]^{\ddagger}$. For the $HCl\cdot CO_2$, $HBr\cdot CO_2$, and $HI\cdot CO_2$ van der Waals complexes, Wittig and co-workers studied product state distributions,[5] and the cluster geometry has now been examined in the infrared studies of Beaudet and Wittig.[7] For the $H+CO_2$ reaction there is thus a considerable body of experimental[2,5,8] and theoretical[9–11] studies aimed at understanding the dynamics. Recent theoretical work by Shin, Wittig, and Goddard[9] has highlighted the influence of the large, highly polarizable halogen atom upon the subsequent course of the reaction. In their *ab initio* generalized valence bond–configuration interaction calculations on the $HBr\cdot CO_2$ system they find that the most favorable pathway for reaction is via a Br–C(O)–OH intermediate where the C–Br bond energy is calculated to be 63.4 kcal mol^{-1}. They explain the relatively cold OH distributions, which they observe resulting from this reaction, in terms of the formation of this intermediate. They also suggest that formation of an analogous transient I–C(O)–OH intermediate could account for the long lifetimes, along with the possible double exponential rise of OH concentration.[2] These studies, while providing information relating to bulk bimolecular reactions, are thus possibly influenced by the presence of a third body.

A solution to this problem which still enables the establishment of a zero of time and subsequent time-resolved "clocking" of the reaction was recently proposed[12] and studied,[3] and is our focus here. The idea is to make the heavier atom or radical in the dissociated precursor the reactive partner, leaving the lighter fragment to rapidly depart from the scene while the bimolecular reaction between the heavier fragment and the other molecular participant in the complex proceeds unperturbed. One advantage of this idea is that it enables a bimolecular reaction to be studied without the perturbation introduced in the earlier studies by the proximity of the halogen atom.

Further advantages include a much lower translational energy imparted to the reactive system, making it more sensitive to features of the underlying potential surface. In addition, the range of effective impact parameters is even more limited than in the case of a light precursor, due to smaller vibrational motions of the heavy precursor in the van der Waals cluster, and the low energy imparted from the initial photodissociation (*vide infra*). To deduce the impact parameter range, the geometry and large amplitude motions of the van der Waals precursor complex must still be known.

B. The $Br+I_2$ reaction and related systems

The reaction $Br+I_2 \rightarrow BrI+I$ is calculated to be exoergic by 6.7 kcal mol^{-1} (ΔH^0_{298} from bond strengths[13]). While a direct measurement of the rate of this reaction awaits determination, a pioneering crossed molecular beam study of this reaction was carried out by Lee, McDonald, LeBreton, and Herschbach.[14] For an average collision energy in the center of mass frame of ~ 3 kcal mol^{-1} they found product IBr scattered to wide angles, and they concluded that there is little or no activation barrier to reaction, with the dominant short-range interaction being attractive. Furthermore, they proposed an "osculating complex" model[15] with a mean complex lifetime of ≈ 5 ps, and estimated the well depth for the $[BrI_2]^{\ddagger}$ to be $\geqslant 10$ kcal mol^{-1}. This estimate for the lifetime is based on a number of assumptions which will be discussed below. However, the main points of relevance to this study are that the reaction proceeds on an essentially attractive potential energy surface via the formation of a long-lived intermediate complex. Further work by McDonald[16] reports the product translational energy distribution, which was analyzed using the osculating complex model.

A subsequent crossed beam study by Loesch and Beck[17] in which they measured angular product distributions for $Br+I_2$ under similar conditions is in good agreement with the work of Lee *et al.*[14] They investigated the reactions $Cl+Br_2$, $Cl+I_2$, Cl+BrI/IBr, and $Br+I_2$, following the earlier study of Beck *et al.* on the $Cl+Br_2$ reaction.[18] They observed predominantly forward scattering in $Cl+Br_2$, I_2, and BrI ($\rightarrow ClBr+I$), increased backward intensity for $Br+I_2$ and nearly forward–backward symmetric scattering for Cl+IBr ($\rightarrow ClI+Br$), attributing this to a variation (in increasing order) of reaction time for these systems. They also observed energy partitioning favoring internal degrees of freedom and concluded that these reactions proceed with little or no activation barrier.

The halogen atom–molecule exchange reactions have been widely studied by crossed molecular beam techniques,[14,16–32] and were among the first to have been successfully investigated using "universal" crossed molecular beam machines with mass spectrometric detectors.[29] These reactions have relatively large cross sections (4–40 Å^2)[33]

and appear to be dominated by attractive forces with little or no barrier to reaction.[33] Many of these, in particular F+XY reactions, have been studied by Grice and co-workers, both by crossed beam methods and theoretically.[23–28] As observed by Grice and co-workers,[23–28] Loesch and co-workers,[17,18] and other groups,[19–22] the reaction dynamics vary from "long-lived" collision complexes (e.g., $Cl+IBr$,[17,19,22]) via osculating complexes (e.g., $Br+I_2$,[14,17]) to direct for most of the other systems studied (e.g., $Cl+Br_2$,[14,16–21,29] or $Cl+I_2$,[28]). In their study of the $Cl+Br_2$ reaction Valentini, Lee, and Auerbach[29] did conclude from their product recoil energy distributions at three collision energies that *neither* an osculating complex model *nor* a spectator stripping one fully describes the observed dynamics, which seem to change from complex to stripping as the collision energy is increased.

If a complex is long lived, a "stable" trihalogen intermediate will be formed. In the gas phase, trihalogen radicals have long been understood to be important in halogen atom recombination reactions. The unusual efficiency of I_2 as a third body in I atom recombination was attributed by Bunker and Davidson[34] to the formation of a stable (by 5.3 kcal mol^{-1}) I_3 species. Porter[35] presented evidence in support of the species. More recent gas phase kinetic studies[36–38] have also invoked a stable I_3 complex to explain experimental observations. Br_3 was observed in the gas phase by Sigrist *et al.*[39] as a result of $(Br_2)_2$ photodissociation, and Cl_3 was detected by laser-induced luminescence during Cl atom recombination in a study by Kawasaki, Sato, and Inoue.[40]

In their early crossed molecular beam study,[19] Lee *et al.* comment on the stability of various trihalogen radicals, noting that radicals with the least electronegative atom in the central position are the most stable. In later crossed beam studies of diatomic halogen reactions,[41–43] Lee and co-workers actually observed I_2F and ClIF resulting from an endoergic bimolecular reaction of F_2 with I_2 and ICl. Crossed beam studies of the $F+I_2$ reaction by Grice and co-workers,[23–27] along with LIF product distribution studies by Trickl and Wanner[30] and Girard *et al.*[31] have indicated the formation of a relatively long-lived FI_2 intermediate in which F atom migration takes place. In a very recent crossed beam study, Girard *et al.*[32] were able to measure vibronic state-resolved differential cross sections for this reaction, and their overall results are compatible with FI_2 complex formation.

A number of trihalogen intermediates have been observed in matrix isolation studies, principally ClF_2,[44–48] and general agreement exists over a bent geometry with a F–Cl–F bond angle of $\geqslant 136°$.[45,47] Cl_2F, BrF_2, Br_2F, and possibly FI_2 have also been seen in a matrix, but earlier reported observations of Cl_3 by Nelson and Pimentel[49] and Br_3 by Boal and Ozin[50] were later reassigned to their respective negative ions by Wight, Ault, and Andrews,[51] as indicated by Jacox.[52] Several theoretical studies on the structure of the ClF_2 radical have been performed (e.g., Refs. 53–56), and there is now agreement over a bent geometry with an FClF bond angle of $\sim 150°$.

Direct kinetic measurements on halogen atom–molecule exchange reactions have been pursued in parallel with crossed molecular beam studies by a number of groups, driven in part by the need to provide independent determinations of integral reaction cross sections, which are difficult to measure accurately in crossed beam systems.[57] Extensive studies by Clyne and co-workers of the kinetics of F atom[58,59] and Cl atom[57,59,60] reactions with halogen and interhalogen molecules show near collisional rates for almost all of these systems, consistent with reaction on an attractive potential energy surface with little or no barrier to complex formation. As expected, the rates increase gradually as the molecular partner is varied down the periodic group. Br atom kinetics have been less widely studied. Strattan and Kaufman[61] measured the rate of reaction with F_2 finding a value of 1.06×10^{-16} cm^3 $molecule^{-1}$ s^{-1} at room temperature, in accord with the other anomalously slow reaction rates of molecular fluorine with many atoms. An isotopic study of the $Br+Br_2$ reaction by Zaraga, Leone, and Moore[62] gave a rate constant of 4×10^{-11} cm^3 $molecule^{-1}$ s^{-1} at room temperature, and Haugen, Weitz, and Leone[63] found a rate constant of 4.6×10^{-11} cm^3 $molecule^{-1}$ s^{-1} for the reaction $Br+IBr\rightarrow Br_2+I$. In view of the observed trends, we expect that the room temperature rate constant for the reaction $Br+I_2\rightarrow IBr+I$ studied here will be rapid, within a small factor of the collisional rate, consistent with its occurrence on an attractive potential energy surface with little or no barrier to complex formation.[64]

The influence of spin–orbit excitation on Br atom reactions has been investigated by Leone and co-workers for the reaction $Br+IBr\rightarrow Br_2+I$.[63,65] They found that the ground state reaction proceeded at a rate $\geqslant 40$ times faster than the total rate of Br ($^2P_{1/2}$) (Br*) quenching and reaction with IBr. Comparison of the rate of the ground state reaction $Br+Br_2$ of 4×10^{-11} cm^3 $molecule^{-1}$ s^{-1} (Ref. 62) with that of the quenching+reaction rate for Br^*+Br_2 of 1.2×10^{-12} cm^3 $molecule^{-1}$ s^{-1} at room temperature determined by Wittig and co-workers[66] gives a similar factor of ~ 40. Wiesenfeld and Wolk studied the kinetics of the deactivation of I* by Br_2 (Refs. 67, 68) and found that the predominant product of this reaction is spin–orbit excited Br*. Gordon *et al.*[69] have also studied spin–orbit effects in halogen atom–molecule reactions including the reaction $Br+IBr\rightarrow Br_2+I$, and proposed a conservation rule for the spin–orbit excited state, whereby the atomic spin–orbit state is not changed during the stay in the chemically bonded intermediate state. Thus the reaction of Br* with I_2 would be expected to be highly disfavored in comparison with the ground state reaction, as the pathway with spin–orbit conservation is endoergic due to the large spin–orbit splitting of I, as is found in these studies for the parallel reaction $Br+IBr\rightarrow Br_2+I$. Therefore any reaction with spin–orbit excited Br atoms may be discounted in the present study.

C. The technique

The reaction is initiated by a uv pump laser pulse at 218 nm which causes photodissociation of the HBr precursor molecule, and IBr product is probed by LIF at 716.5

nm. HBr absorption in the near uv peaks near 180 nm and drops to a value of ~ 80 liter mol^{-1} cm^{-1} by 218 nm.[70,71] The photolysis wavelength chosen for this study was a compromise between the efficiency of production of uv light, which falls rapidly in this region with decrease in wavelength, and the falloff in absorption coefficient of HBr as the wavelength is increased.

Photodissociation of HBr at 193 nm produces $\sim 15\%$ of Br atoms in the $(^2P_{1/2})$ spin–orbit excited state.[72–74] While this proportion has not been measured for photolysis at 218 nm, it may be reasonable to assume by comparison with HI photolysis[74] that it will still be below 50% at this wavelength. Furthermore, as discussed above, reaction of I_2 with spin–orbit excited Br* to yield ground state products is highly disfavored, and so can be discounted.

The HBr bond strength is listed as 87.56 kcal mol^{-1},[13] leaving an excess energy after absorption of a 218 nm photon and dissociation of 15 250 cm^{-1}. Considering only the $(m=79)$ isotope of Br for simplicity, momentum conservation dictates that the Br atom will receive only 1/80 of the total energy for HBr photodissociation, and 2/81 of the total for DBr, i.e., 191 and 376 cm^{-1}, respectively. This corresponds to Br atom velocities of 2.4 and 3.4 Å ps^{-1}, respectively, and complementary H and D atom velocities of 190 and 130 Å ps^{-1}, indicating that the H or D atom is well clear of the reaction zone while complex formation and decay proceed.

The structure of the $HBr \cdot I_2$ van der Waals complex remains as yet undetermined. Klemperer and co-workers have determined the structure of the $HF \cdot Cl_2$ (Ref. 75) and HF·ClF (Ref. 76) complexes by the molecular beam electric resonance technique. They find in both cases an antihydrogen bonded structure with a linear arrangement of the three heavy atoms. The trend for the van der Waals interaction of the heavier homologues (due to the higher polarizability of the homonuclear diatomic), suggests that $HBr \cdot I_2$ is also expected to have the same basic linear, antihydrogen bonded structure. In any case, the energetics (low translational excitation of Br and van der Waals bonding) are such that there must be a $Br+I_2$ reactive channel for any precursor geometry, and only this channel is probed by the combination of laser wavelengths and filtered fluorescence used here, even if the H position is not exactly known.

The position of the light hydrogen atom is less easily predicted. Klemperer and co-workers determine an *average* H–F–Cl angle of 125° in the deuterated and undeuterated case. However, there is a large amplitude motion due to the bending vibration. For the case of HF·ClF,[76] Klemperer and co-workers concluded a bent equilibrium geometry (angle 125°) from the similarity of HF·ClF and DF·ClF dipole moments. While extrapolation of these results to $HBr \cdot I_2$ should be viewed with caution, it is important to note that the exact H–Br–I bond angle is not as critical in this case due to the proximity of the reagents and the low energy nature of the collision. Such is not the case in $XH \cdot CO_2$ (X=Cl,Br,I) hot-atom studies. The structural effects on the impact parameter are highlighted in Fig. 1 for several types of geometries, including crossed-beam, linear van der Waals cluster, the hydrogen off-axis, and a hypothetical hydrogen-bonded cluster.

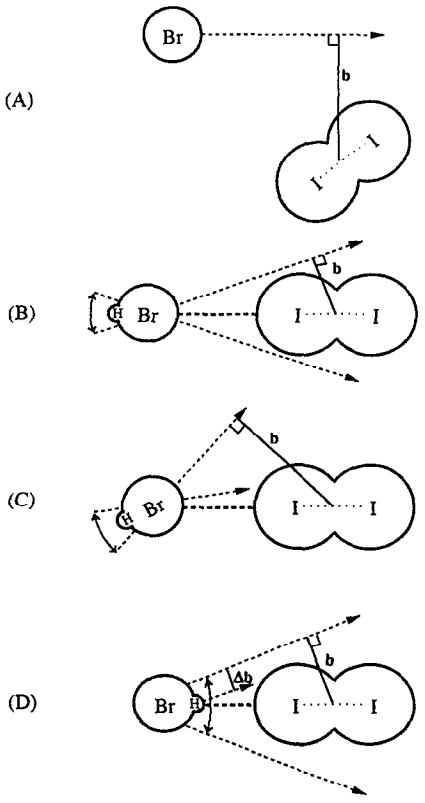

FIG. 1. Schematic showing the effect of different impact geometries on the impact parameter distribution; (A) crossed beam conditions, often leading to large impact parameters; (B): linear $HBr–I_2$ cluster; the displacement of the Br is negligible compared to the effect on its momentum vector due to the hydrogen large amplitude motion; (C) H off-axis linear $HBr–I_2$ cluster shows a somewhat increased impact parameter range; (D) hypothetical hydrogen-bonded configuration for reactive $H+I_2$; note that the impact parameter of the hydrogen is influenced by its position as well as its momentum vector, as opposed to the Br, where only the momentum vector contributes significantly; this adds an additional Δb to the impact parameter; also note that in this configuration, the H would lead to an undetectable reaction or quickly depart, whereas the Br is still trapped. For configuration (D), a reactive $Br+I_2$ encounter requires a turning around of the Br toward the I_2.

For a linear, antihydrogen bonded complex structure of $HBr \cdot I_2$, the translational energy available for reaction can be calculated in the I_2–Br center-of-mass frame from the initial Br atom translational energies derived above. This amounts to 145 and 286 cm^{-1} for $HBr \cdot I_2$ and $DBr \cdot I_2$, respectively (neglecting effects of the van der Waals well discussed later). In contrast, the crossed molecular beam studies employ available energies of the order of 1000 cm^{-1}, making them less sensitive to the lower energy features of the potential energy surface.

IBr product is probed by LIF via the $A\,^3\Pi_1(v'=21) \leftarrow X\,^1\Sigma^+(v''=1)$ transition at 716.5 nm, as observed by Selin.[77] Off-resonance fluorescence from this absorption is expected to lie principally to the red at 730 and 745 nm $(v'=21,v''=2,3)$. The $(A–X)$ system has also been studied by Brown,[78] but attention has primarily been

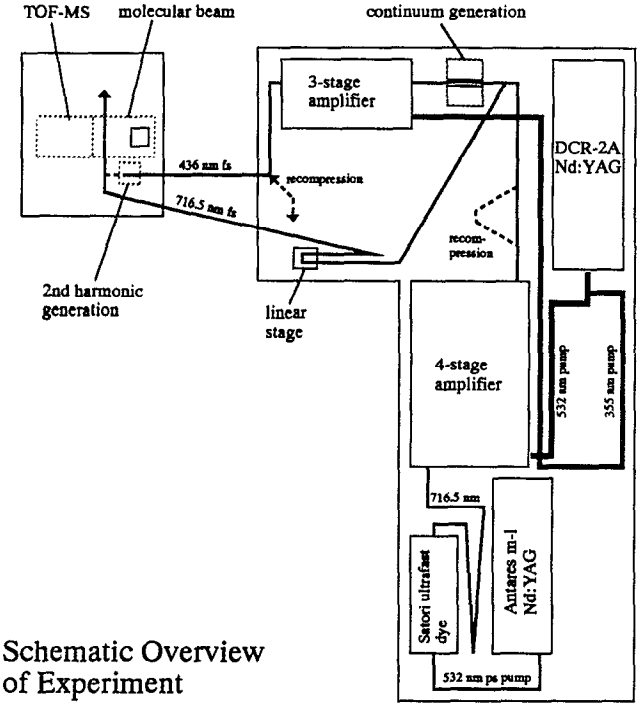

FIG. 2. Overview of the experimental arrangement, showing the generation of the fs laser pulses, their amplification and subsequent manipulation, and the molecular beam and TOFMS.

focused on the visible (B–X) system, and a number of LIF studies have been carried out.[79–82] The $B\,^3\Pi(0^+)$ state of IBr is extensively predissociative,[80–83] and is not expected to play a role in the current study.

Our simulations of jet-cooled LIF spectra for I_2 in the 716.5 nm region indicate that there is no appreciable interference, and similarly the pump laser wavelength of 218 nm lies in a "window" in the I_2 absorption spectrum (see, e.g., Refs. 84–87) at wavelengths longer than the $D(0_u^+)\leftarrow X(0_g^+)$ absorption band in the 176–200 nm region.

III. EXPERIMENT

The essential elements of the experimental arrangement can be classified into four main areas: generation of the ultrafast pump and probe laser pulses; characterization of the laser pulses and establishment of the zero of time; formation and characterization of the $HBr\cdot I_2$ complex; and LIF collection and signal processing. A simplified schematic overview of the experimental setup is shown in Fig. 2.

A. Generation of the ultrafast pump and probe laser pulses

The scheme for the generation of μJ level fs pump and probe laser pulses is shown in Fig. 2. A mode-locked Nd:YAG laser (Coherent Antares 76S) was used as the primary ultrafast pump source. It generated $\sim$50 ps 30 nJ pulses of 532 nm light after second harmonic generation, at a repetition rate of 76 MHz, and a cw power of $\sim$2 W. This was used to pump an ultrafast dye laser (Coherent Satori) of the linear cavity, synchronously pumped design, employing twin jets (gain and saturable absorber), and dispersion compensated via a prism pair. Both directional and amplitude stabilization devices were employed on the pump beam and this, combined with active stabilization of the cavity length, ensured stable and uninterrupted operation over the long periods necessary for accumulation of the experimental transients. A single plate birefringent filter was employed to provide wavelength selection. The gain medium was LDS722 (Exciton) in ethylene glycol, and the saturable absorber used was DDI (Exciton) in ethylene glycol. The laser was set to a wavelength of 716.5 nm, yielding 150–200 mW of light with a pulse autocorrelation of $\sim$350 fs. It was operated with this somewhat longer pulse to ensure stable operation, once the long (by the standards of this equipment) time scale of the $Br+I_2$ reaction had been established.

The $\sim$2 nJ 716.5 nm pulses were amplified in a four stage amplifier pumped by 532 nm ($\sim$6 ns FWHM) light from a Q-switched Nd:YAG laser (Spectra Physics DCR-2A with filled-in beam option) operating at a 20 Hz repetition rate. The laser beam was introduced into the first stage after an optical delay of about 3 m in order to eliminate ASE (amplified spontaneous emission) resulting from back reflection off the Satori's output coupler. LDS750 (Exciton) laser dye in methanol was used in the first stage, followed by LDS722 (Exciton) in methanol in the last three stages to minimize ASE. The first three stages were side pumped, and the final stage end pumped. The beam was focused through a 125 μm pinhole between the first and second stages: further precautions against ASE were found to be unnecessary. The beam was expanded between each of the stages reaching a diameter of 0.5 cm in the last stage. The 20 Hz amplified pulse energy was estimated to be $\sim$60 μJ with $\sim$20 μJ of ASE. For this experiment pulse recompression was not used, though facilities do exist for this using prism pairs.

The amplified beam was split using a pellicle beam splitter (Melles Griot uncoated 10% R/90% T or coated 30% R/70% T). The less intense reflected probe beam passed across to the optical delay section where it underwent one or two retroreflections off appropriate reflectors mounted on a computer controlled linear stage (Micro Kinetics, 25 mm excursion, 0.1 μm resolution). This in turn was mounted on a much longer low resolution manually controlled stage (Micro-Contrôle) which facilitated location of the zero of time. After this variable optical delay, which required careful alignment to avoid problems of beam walk off, the beam passed across to the molecular beam where it was focused into the reaction zone using a 50 cm fl (focal length) plcx (planoconvex) lens.

The stronger, transmitted component of the 716.5 nm beam was focused into a 1 cm path length cell containing D_2O (Aldrich). This provided a white light continuum, which was recollimated and directed through a 460 nm, 10 nm FWHM interference filter (Corion) tilted to shift its center wavelength to 436 nm. The resulting low intensity beam (estimated pulse energy $\sim$50 nJ) was reamplified in

a three stage amplifier side pumped by 355 nm laser light from the Q-switched Nd:YAG laser. This amplifier was similar in design to the first one, except that it lacked the final, end-pumped stage. The dye used was coumarin 440 (Exciton) in methanol, and the radical scavenger diazabicyclo[2.2.2]octane (DABCO; Kodak) was added to prolong the dye lifetime. Even so, initial experiments were hindered due to a dye lifetime of 1 h or less: increasing the dye volume, purging the solutions with nitrogen and minimizing the 355 nm pump laser intensity together enabled continuous runs of 12 h or more, however.

The pulse energy of the second amplifier was measured as $\sim 40\,\mu$J amplified light and $\sim 20\,\mu$J ASE (the latter was essentially eliminated in the frequency doubling process). Again, pulse recompression, while provided for, was not used at this stage. The 436 nm beam passed over to the molecular beam apparatus, where the second harmonic was generated using a 300 μm thick BBO crystal (β-barium borate; Cleveland Crystals) placed about 1 cm before the focus of a 15 cm lens. The doubling efficiency at this wavelength appeared to be quite low, and the estimated pulse energy at 218 nm was 1 μJ. An interference filter transmitting 35% at 218 nm (Acton Research) was used to check the intensity of the uv beam by blocking the fundamental. It was not used during the experiments in order to maximize the signal: tests were carried out with the residual 436 nm beam present to ensure that this had no influence on the results. The 218 nm beam was recollimated and focused into the chamber via a 50 cm fl plcx uv lens after reflection off a dichroic beam combining optic.

The two beams were aligned through the chamber and then focusing and overlap were checked by deflecting the beams into an external 150 μm pinhole via a removable Al coated mirror. The beams entered and exited the molecular beam chamber via baffle arms containing electroformed conically tapered baffles to minimize scattered light from the windows. The entrance window comprised a 1 in. diameter 0.025 in. thick optically flat sapphire plate, with a 0° optic axis oriented for normal incidence with no birefringence, and MgF_2 antireflection coated (Meller Optics). Both beams entered the apparatus with vertical polarization.

B. Characterization of the pulses and the zero of time

The pulse width of the unamplified 716.5 nm beam was monitored by a real-time scanning autocorrelator of the rotating mirror type, built in this lab and similar to that described by Yasa and Amer.[88] Pulse widths of ~ 350 fs were observed. The frequency tuning of the laser was controlled with reference to a monochromator/PMT set to 716.5 nm. The amplified beam pulse autocorrelation was determined using the linear stage and a 100 μm KD*P crystal; a FWHM of 380 fs was observed.

The main method used for characterizing the laser pulses was cross correlation between the 218 nm pump and the 716.5 nm probe. This was achieved[89] using (1+1) photoionization of N,N dimethylaniline (Kodak) in a small ionization cell with an entrance window identical to the one on the reaction chamber, antireflection coated in the same batch. After alignment of the beams through the external pinhole this cell was placed just in front of the focus, and a 9 V bias applied across the electrodes. The current passing was amplified by a sensitive current-to-voltage converter (Keithley), and monitored by a boxcar integrator (PAR) interfaced to a computer.

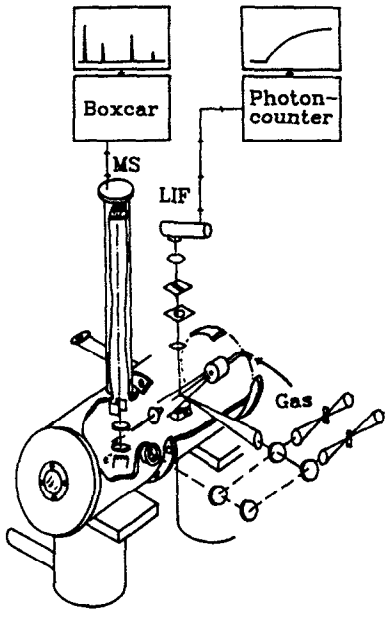

FIG. 3. The molecular beam system, showing the interaction region 2 cm from the pulsed valve below the LIF detector, and the EI-TOF mass spectrometer used to characterize the cluster concentrations.

Cross correlations were obtained by recording this signal as a function of translation stage position, and converting position to time delay via a previous calibration. The signal obtained was a combination of a very small steady state "step function" signal combined with a much larger peak. Presumably the transient nature of the signal was due to extremely rapid IVR (intramolecular vibrational relaxation) within the molecule. Initial experiments with a recompressed 716.5 nm beam gave shorter cross correlation widths than were later determined for pulses used in the experiments described here, and so we are confident that the ionization peak well represents the cross correlation function of the two pulses, as well as providing an accurate indication of the zero of time, when the pump and probe pulses overlap. Spectra of the 716.5 and 436 nm beams yielded a time-bandwidth product 2–3 times the transform limit, due mainly to lack of recompression. It was not possible to take the spectrum of the 218 nm pump beam; its frequency bandwidth would be reduced with respect to the 10 nm FWHM 436 nm beam due to the limited acceptance angle of the BBO doubling crystal.

C. Formation and characterization of the $HBr \cdot I_2$ complex

The molecular beam apparatus used is shown in Fig. 3; only the differences to the setup described previously[2] will be reported in detail here. The beam was constructed of two main cylindrical chambers separated by a skimmer, and each pumped by a separate diffusion pump and cryobaffle, backed by a single high throughput rotary pump. The primary chamber, which was operated at a pressure of 10^{-4} Torr or less during experiments, was arranged with the nozzle, laser entrance and exit baffle arms and LIF collection optics on three mutually orthogonal axes. The skimmed molecular beam passed into the second chamber which contained the time-of-flight mass spectrometer (TOFMS), and was operated at a pressure of typically 10^{-6} Torr.

The heatable nozzle assembly (General Valve) consisted of a solenoid actuated stainless steel piston which mated with a 0.5 mm orifice in a Rulon polymer insert which was screwed into a face plate. A channel in the plate led from an external chamber containing the I_2 to the gas stream just before the orifice. Two heating elements and a thermocouple mounted on this plate enabled the whole assembly to be maintained at 160 °C via an external temperature controller (Omega). It is estimated that the temperature of the I_2 reservoir, which was in good thermal contact with the face plate, would have been 10–20 °C below that of the main assembly, thus ensuring that the valve did not clog with condensing I_2.

The valve was operated in synchronization with the laser pulses at a repetition rate of 20 Hz. Both the duration and predelay of the gas pulses with respect to the lasers were adjustable externally, and it was found that the clustering efficiency was very sensitive to these adjustments. The valve was operated with a ~ 400 μs pulse, and the time delay between the opening of the valve and the arrival of the laser pulses adjusted to optimize the concentration of the cluster at that time. He (Liquid Air) and HBr (Matheson) or DBr (99% isotopic purity; Cambridge Isotope Laboratories) were supplied from an external gas mixing manifold where their flows were limited by mass flow controllers (MKS), to a ratio of typically 3 sccm (standard cubic centimeters per minute) H(D)Br to 20 sccm He, though this was adjusted to maximize the $HBr \cdot I_2$ cluster signal. The backing pressure was monitored by a 5000 Torr capacitance manometer (MKS Baratron), and was typically in the range 1800–2600 Torr.

The electron impact time-of-flight spectrometer (EI-TOFMS) arrangement has been described previously:[2] in these experiments a microchannel plate assembly constructed in this laboratory was used instead of the former electron multiplier, and the length of the flight tube increased from 1 to 1.2 m. The 50 Ω terminated signal from this detector was amplified by two stages of a wide bandwidth amplifier ($\times 5$, 300 MHz; SRS) and fed into the input of a gated photon counter (SRS) which was computer interfaced and operated in the scan mode to collect a mass spectrum. A typical example after optimizing for $HBr \cdot I_2$ concentration is shown in Fig. 4.

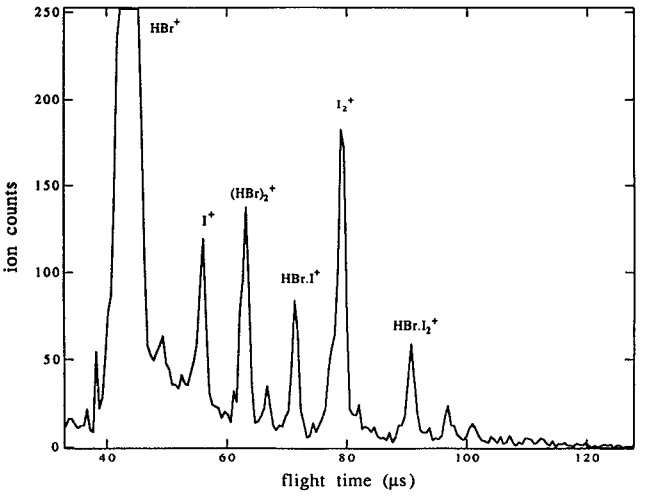

FIG. 4. Time-of-flight mass spectrum obtained under typical operating conditions. The TOFMS deflection plates were set to bias for higher mass, and only the range from $m/e \sim 80$ and above is shown for clarity.

D. LIF collection and signal processing

The laser beams, focused to an approximately 300 μm beam waist, intersected the molecular beam approximately 20 mm downstream of the nozzle, corresponding to an X/D of 40. Fluorescence was collected by a 5 cm diameter f/1.5 Suprasil plcx lens aided by a 4 cm diameter, 2.4 cm focal length concave parabolic mirror placed below the beams. The emission passed through a Schott RG9 filter to block light to the blue of ~ 720 nm. It was estimated that on-resonance LIF at 716.5 nm along with laser probe scatter would be cut by $\sim 50\%$, but background scatter and fluorescence resulting from the 218 nm pump beam would be cut dramatically. Another plcx lens (5 cm diameter, f/1.5) focused the fluorescence onto an adjustable slit to further discriminate against scattered light. Another f/1.5 lens recollimated the light and a final f/1.5 lens focused it onto the photocathode of a GaAs single photon counting PMT (Hamamatsu R943-02, chosen because of its high efficiency in the near infrared), mounted within a thermoelectrically cooled housing (Products For Research).

The 50 Ω terminated output of the PMT was amplified in the same way as the TOFMS signal and fed into the gated photon counter. A fast photodiode mounted behind one of the 532 nm Q-switched Nd:YAG laser turning mirrors provided the trigger pulse, and the gate was set to count typically from 0.5 to 3.5 μs after the arrival of the laser pulses. The counts were accumulated for between 20 and 40 laser shots and fed to an IBM PC-AT computer which also controlled the linear stage.

E. Signal optimization

After optimization of pump and probe laser beam intensities and overlap, $HBr \cdot I_2$ mass spectral intensity and pulsed valve delay time and width, a total photon count rate of 1–2 per pump/probe laser shot was obtained. Final optimization was carried out while monitoring the count

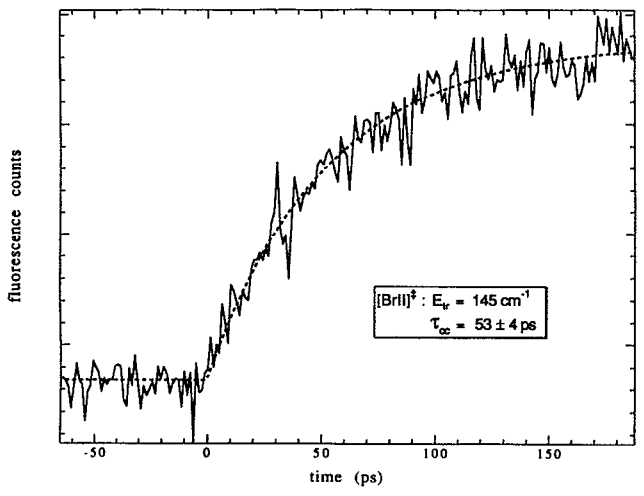

FIG. 5. Experimental transient showing the time-resolved formation of IBr from the reaction $Br+I_2 \rightarrow BrI+I$ starting from an $HBr \cdot I_2$ complex, as monitored by LIF. The data fit a rising exponential as indicated, with the zero of time being fixed by the photoionization cross-correlation (see the text).

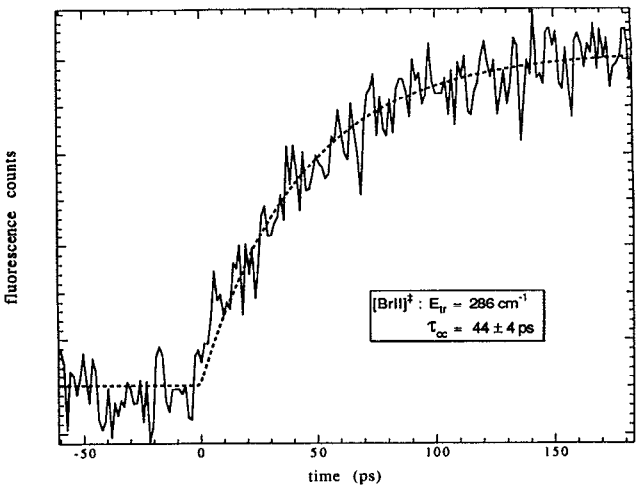

FIG. 6. Experimental transient as in Fig. 5, but starting from a $DBr \cdot I_2$ precursor, showing a faster rise time.

rate with the optical delay set to its maximum value for the combined pump/probe beams.

The background was found to arise almost entirely from the uv pump beam, rather than the red probe beam or residual 436 nm fundamental of the doubled pump beam. While it does appear that the uv pump wavelength of 218 nm is in a window in the I_2 absorption spectrum, at these low count rates and high overall I_2 concentrations even a very small absorption cross section could result in such a background. This background signal was also observed with no HBr present. Girard *et al.*[31] observed intense fluorescence at wavelengths below 495 nm using a supersonic I_2 beam, but found this to be much reduced in a quasieffusive beam, attributing this effect to $(I_2)_2$ formation. In our early experiments[3] we were able to detect some $(I_2)_2$ in our mass-spectral scans, and an experimental transient with a rapid rise time of ~ 5 ps was obtained with I_2 alone. However, under the optimized conditions employed here, no $(I_2)_2$ mass spectral peak could be seen, and no enhancement of signal over background was observed with I_2 alone.

To trace the origin of the signal to the $HBr \cdot I_2$ van der Waals cluster, enhancement was monitored as a function of the monomer, dimer, and multimer concentrations. Enhancement was not observed with I_2 or HBr alone, and was found to be very sensitive to the concentration of $HBr \cdot I_2$ cluster as observed by TOFMS with both I_2 and HBr present, but at low ($<15\%$ of $HBr \cdot I_2$) concentrations of larger clusters, confirming its origin from the mixed dimer.

IV. RESULTS AND DISCUSSION

A. The lifetime of the collision complex

Our results for $HBr \cdot I_2$ and $DBr \cdot I_2$ are presented in Figs. 5 and 6, and comprise weighted composites of several scans. Risetimes τ_{cc} (assumed to be single exponential, see below) of (53 ± 4) and (44 ± 4) ps, respectively, were determined using nonlinear least-squares analysis of the data, standard deviations being quoted at the $\pm 2\sigma$ level. All individual scans also showed this risetime difference. The DBr precursor reaction, leading to more energetic Br atoms, is seen to be significantly faster than the HBr precursor reaction. With better S/N, these transients may show nonexponential (fast and slow) behavior and/or quantized steps (see below).

These observations provide direct information about the collision complex: (1) The triatomic species $[BrII]^{\ddagger}$ is very stable on our (femtosecond) time scale, reflecting a "sticky" collision in the $Br+I_2$ encounter. (2) The observation indicates the presence of a well in the transition state region, capable of supporting a stable BrII molecule, and an exit channel barrier (see below) which significantly affects the threshold dynamics. (3) There is no entrance channel barrier, as evident from the threshold measurements and discussed below.

In the coming sections we shall focus our attention on the nature of bonding, the PES, the dynamics (via classical trajectories), and comparison with other methods for studying the dynamics.

B. Bonding in the collision complex

Parallel to experimental investigations, halogen atom–molecule exchange reactions [A+BC] have received a considerable amount of theoretical attention. For some of the lighter trihalides, ground and excited electronic states have been calculated at the SCF or CI level.[55,56,90] For the heavier trihalides (X=Br,I), various semiempirical methods have seen continued application, due to the difficulties in dealing with many-electron systems by more rigorous methods.[54,91–95] For Br and I, spin–orbit coupling is an important contribution to the electronic energy, resulting in large splittings between electronic states that would otherwise be degenerate. Nonetheless, only the I_3 system has been studied by a relativistically corrected calculation.[96] In

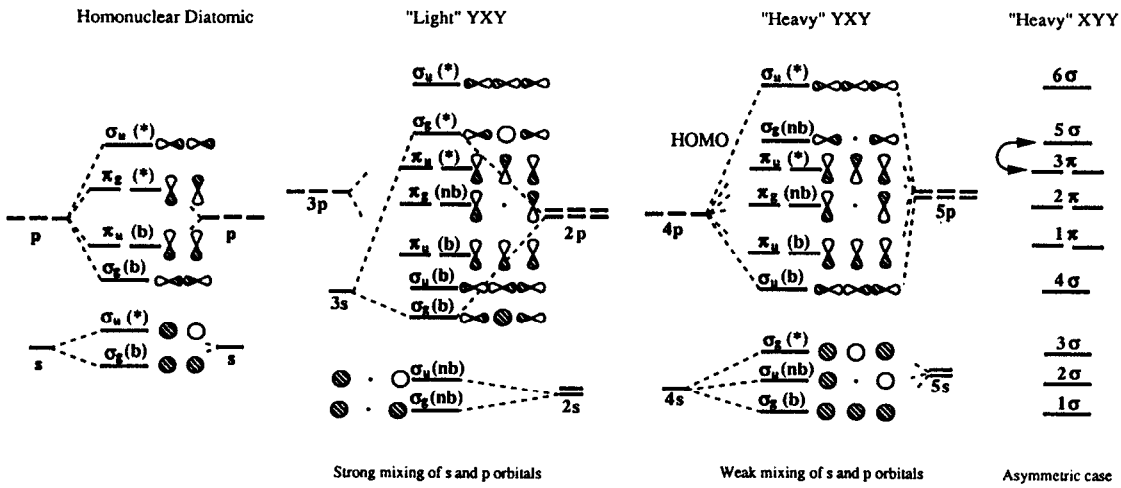

FIG. 7. Schematic orbital diagram for various trihalogen systems. All relativistic corrections have been neglected, which would lift the degeneracy of the π orbitals. On the left is shown the standard correlation diagram for a homonuclear diatomic with more than half-filled p shell, as applicable to I_2. The next diagram shows the formation of a light symmetrical halogen complex, with notable s and p mixing; the third correlation diagram corresponds to the case of heavier halogens, where the amount of s and p mixing is decreased. For the asymmetrical complex case, such as BrI_2, the last diagram shows the orbital numbering used in the text; the orbitals are now asymmetrical, and the 3π and 5σ orbitals may be shifted in order.

what follows, we shall first consider a nonrelativistic schematic of the contributing orbitals, which will then be followed by some more detailed considerations.

Consider the approach of a bromine atom ($4s^24p^5$) to an iodine molecule ($n=5$ valence shell) to form an open-shell 21 electron triatomic system. For the diatomic I_2, the MOs are the usual linear combinations of valence s and p orbitals (Fig. 7), which form the configuration $\sigma_g^2(s)\ \sigma_u^{*2}(s)\ \sigma_g^2(p_z)\ \pi_u^4(p_{x,y})\ \pi_g^{*4}(p_{x,y})$. The HOMO of the halogen molecule is therefore the π_g^*, while the LUMO is the σ_u^* (p_z). The MOs of the complex BrI_2 (or more generally XY_2) form depending on the relative energies of the ns and np orbitals for X and Y. For light systems (e.g., ClF_2 in Fig. 7) the $2s$ orbitals of the F atoms are separated in energy, but the $3s$ orbital of the Cl atom is fairly close in energy to the fluorine $2p$ orbitals (Fig. 7). Accordingly, there is extensive mixing between the chlorine $3s$ and the fluorine $2p_z$ orbitals. The MOs take on the form familiar in the literature,[23] and the odd electron resides in the σ_g^* orbital. The bond order can be deduced by considering the nature of the orbitals [bonding (b), antibonding (*), or nonbonding (nb)] and in this case it is 1.5 (larger than the initial bond order of unity in F_2+Cl). The LUMO will be of interest later in discussions of the frontier orbitals.

In "heavier" systems (e.g., IBrI), the ns orbitals are closer together and the s–p mixing is not as large. Consequently, the s orbital subsystem will mostly mix separately from the p subsystem. The MO's of the complex are shown in Fig. 7. The nature of the (b), (*), or (nb) character of the orbitals changes, and in fact for the same 21 valence electron system, the bond order could range from unity [if the σ_g(nb) lies at higher energy than the π_u^* orbital] to 1.5 (in the reverse case). For asymmetric systems like BrI_2, the u and g symmetry labels are no longer valid, and a general numbering of the orbitals (which may now have

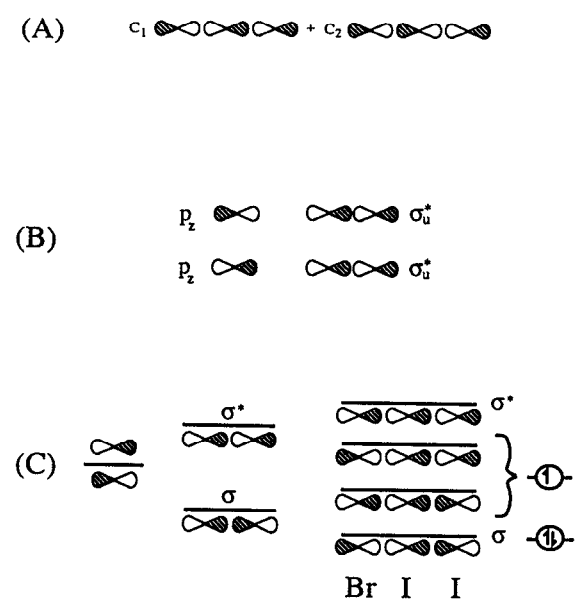

FIG. 8. P_z orbital interaction possible as Br approaches I_2; refer to the text for a detailed discussion of the frontier orbital picture.

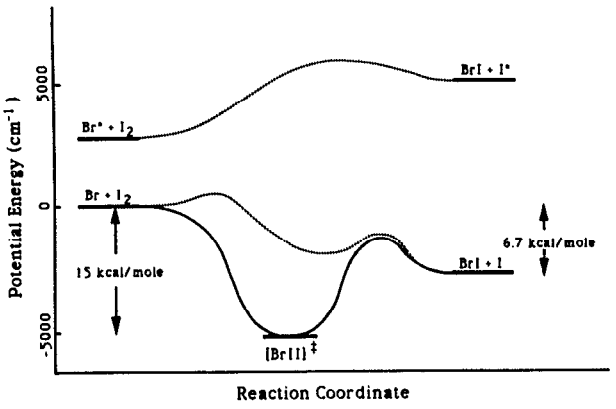

FIG. 9. Reaction coordinate showing the effects of spin–orbit splitting. The three approaches of the Br p orbital to I_2 lead to three surfaces, of which only the lowest should play a major role in the present experimental investigation. Note that crossing from the Br/I to the Br*/I* surface is forbidden by a propensity rule. The exoergicity and well depth are also noted in kcal mol^{-1}.

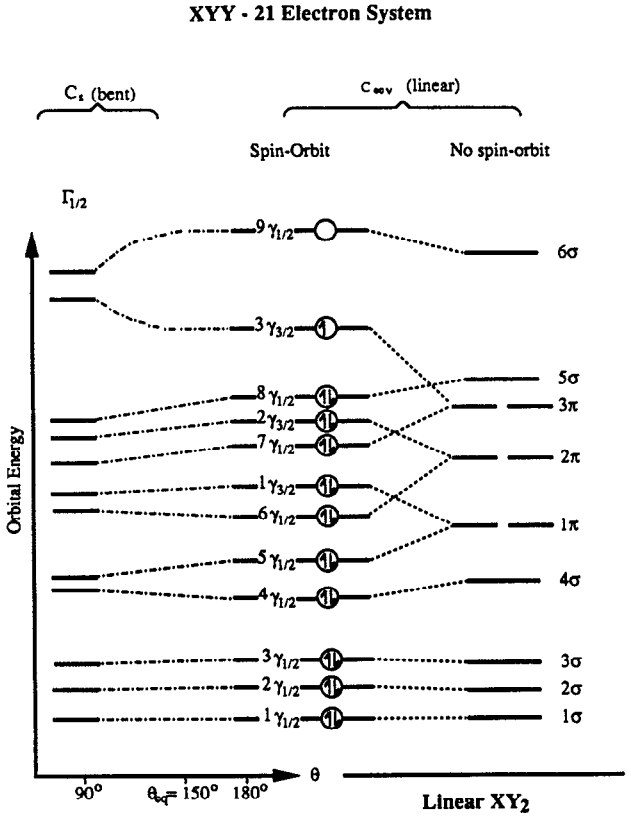

FIG. 10. Correlation diagram for the 21 valence electron system BrI_2. On the left are shown the atomic orbitals (4s and 4p for Br, 5s and 5d for I) which make the major contribution to the MO's of the linear complex. It can be seen that the HOMO has antibonding character, yielding an overall bond order of 1.5. (Orbitals are numbered starting in the valence shell) The degeneracies of the π orbitals are lifted when spin–orbit coupling is considered: due to the unpaired electron, π states ($\ell=1$) lead to $\gamma_{1/2}$ and $\gamma_{3/2}$ states, while σ orbitals lead only to $\gamma_{1/2}$ orbitals. Upon bending the molecule to the C_s geometry, the HOMO energy increases; nonetheless, BrI_2 probably has a slightly bent geometry in its electronic ground state, due to the lowering of the 1π orbital energies.

asymmetric shapes discussed below) emerges, as shown in Fig. 7.

For the case of interest to us here ($Br+I_2$), the collinear approach will lead to a complex of the form BrII. The bond order depends on the composition of the 5σ orbital. Since the complex is not symmetric around the central atom, the 5σ orbital can be viewed as a linear combination of two orbitals formed by combining p_z orbitals of all three atoms [Fig. 8(a)], where one of the orbitals is bonding on the I–I and antibonding on I–Br, and vice versa for the second one. When the coefficients $c_1=c_2$ for symmetric systems (e.g., IBrI), the combination yields the nonbonding orbital shown in Fig. 7.

From the above discussion, it appears that the complex bonding in the nonrelativistic limit involves the σ system, and this simple picture is consistent with Fukui's frontier orbital approach.[97] The LUMO of I_2 is the σ_u^*. If we consider the reaction as resulting from a transfer of charge density from the attacking atom Br HOMO (p_z in this case) to the LUMO of I_2, then we have, as shown in Fig. 8(b), the completely antibonding orbital (6σ) and an orbital which is bonding on I–Br and has a node on the I–I (the $c_2=0$ limiting case). (Interestingly, side-on attack is predicted to have a higher energy barrier, neglecting spin–orbit excitation, since the net overlap is zero.) This latter orbital is a good zeroth-order description for the reaction: bond formation (I–Br) and bond breakage (I–I).

Herschbach's description[98] of these halogen reactions in crossed beam experiments is simply to make the σ and σ^* orbitals shown in Fig. 8(c), and one can now see the importance of the frontier orbitals. Furthermore, the analogy between $X+Y_2$ and $h\nu+Y_2$ reactions can now be physically understood: both create a node on the Y–Y bond. The effect of electronegativity of the atoms involved can also be appreciated. Since the LUMO of the halogen molecule is antibonding, the orbital will be localized on the atom least in electronegativity, and the reacting atom will attack at such a point.

These observations are also supported by *ab initio* calculations and more detailed considerations involving spin–orbit coupling; while some of the simpler calculational methods predict saddle points or very shallow wells for X_3 or XY_2,[99–102] more recent (semiempirical/SCF/CI) calculations show that many trihalides have a bound ground state PES with a well-defined equilibrium geometry.[53,55,56,90] Consider Cl_3 as an example: One DIM (diatoms in molecules) study concludes that the molecule has only a saddle point on the ground state surface,[101] while the PES used by Thompson (based on the London equation)[103] shows a small symmetrically located well. LEPS and Sato surfaces from Ref. 102 show behavior ranging from saddle points to deep wells (≈ 8 kcal mol^{-1}). CNDO/2 and INDO calculations indicate a stable symmetric well (or a late well for some XY_2 species),[54,94] as do

TABLE I. Parameters for the optimal potential used in the $Br+I_2$ trajectory calculations described in the text. 28 different-valued parameters were used to describe the three-dimensional surface $V(r_1,r_2,r_3)$; 11 were fixed at values based on or derived from the literature, 13 were fixed at physically reasonable values determined by investigating derivatives and fixed points of the surface, and 4 were adjusted to bring the surface into concordance with the available temporal and scattering results.

Type	Name	Value	Unit	Description
Dissociation energy (DE)	$D_{01}= D_{03}$	14654	cm^{-1}	IBr DE*
	D_{02}	12439	cm^{-1}	I_2 DE
	$D_{11}= D_{13}$	4550	cm^{-1}	DE increase in complex (BrII)
	D_{12}	3270	cm^{-1}	DE increase in complex (IBrI)
	$D_{21}= D_{22}= D_{23}$	-500	cm-1	DE correction linear vs. bent complex
	σ_{D1}	1.2	$Å^{-1}$	DE range parameter
	σ_{D2}	0.5	$Å^{-1}$	DE range parameter
	σ_{D3}	1.4	$Å^{-1}$	DE range parameter
Force constant	$\beta_{01}= \beta_{03}$	4.65	-	IBr Morse force constant
	β_{02}	4.97	-	I_2 Morse force constant
	$\beta_{11}= \beta_{12}= \beta_{13}$	-3.5	-	Force constant change in complex
	$\sigma_{\beta 1}$	1.0	$Å^{-1}$	Force constant range parameter
	$\sigma_{\beta 2}$	0.9	$Å^{-1}$	Force constant range parameter
Bond length	$r_{e01}= r_{e03}$	2.47	Å	IBr equilibrium bond length
	r_{e02}	2.66	Å	I_2 equilibrium bond length
	$r_{e11}= r_{e12}= r_{e13}$	0.28	Å	Bond length change in complex
	σ_{r1}	1.0	$Å^{-1}$	Bond length range parameter
	σ_{r2}	0.4	$Å^{-1}$	Bond length range parameter
General constants	γ	1.5	$Å^{-1}$	Overall range parameter
	$\theta_1= \theta_2= \theta_3$	150	°	Complex near-equilibrium angles
Barriers	$B_{01}= B_{03}$	-2300	cm^{-1}	Exit channel decrease in DE
	$r_{B1}= r_{B3}$	3.9	Å	Exit channel barrier position
	r_{B2}	2.47	Å	Exit channel barrier position
	$\sigma_{B1}= \sigma_{B3}$	0.3	Å	Exit channel barrier width
	σ_{B2}	0.7	Å	Exit channel barrier width
van der Waals interaction	$C_1= C_3$	2.71×10^6	$Å^6cm^{-1}$	Br-I vdW constant
	C_2	3.39×10^6	$Å^6cm^{-1}$	I-I vdW constant
	m	4.5	Å	Range parameter

the available SCF/CI calculations (but the latter did not systematically sample the antisymmetric stretching mode).[90]

The consensus seems to be that the stability increases with heavier atoms, and decreases with the more electronegative atom located centrally in the case of asymmetric clusters, with only the most extreme cases of the latter showing a saddle point. The well is located near symmetrically or possibly "late" in the exit channel of the heavier halogen atom. For several XY_2 clusters, stability has been verified experimentally by the analysis of infrared spectra in matrices,[48] and for others, beam scattering studies strongly suggest a bound ground state.[14,17,41–43]

C. Potential energy surface

Figure 9 represents a schematic view of a cut through the PES along the reaction coordinate and Fig. 10 shows the orbitals (including spin–orbit coupling) of the complex for different bond angles. To relate the dynamics on the PES to the experimental results reported here (real-time studies of the collision complex) and to results reported earlier (scattering studies of the products), more quantitative features of the potential must be considered. Several empirical approaches have been tested in the literature to generate model potentials for A+BC collision studies. One of the earliest models is the LEPS surface for collinear studies, which relies on the London formula. These surfaces have been used to unravel the nature of repulsive and attractive energy release, and the dependence on the location of the transition state along the reaction coordinate.[104] In a different approach, the total potential energy is represented by a sum of "diatomic" Morse potentials, turned on and off at various internuclear distances via the use of a switching function.[105] A representation was also given in terms of a single Morse potential, with the dissociation energies and vibrational frequencies interpolated from reactants to products by a hyperbolic function along the collinear reaction coordinate.[106] For some collinear PESs a Morse potential was rotated about a point along the symmetric stretching coordinate in the r_{AB}–r_{BC} plane, varying the well depth and other parameters as a function of the rotation angle to yield a collinear PES.[107] Some of these PESs have been extended to include the bending mode, although not necessarily in a qualitatively correct global manner.[106]

We have chosen a somewhat different parameterization, which is more easily and symmetrically extended from two to three coordinates, and based on our previous studies of HgI_2 (Ref. 108) and our initial report on BrI_2.[3] Our goals were a fully symmetric treatment of all three diatom+atom limits, and globally correct qualitative (or, if potential parameters can be determined with sufficient accuracy, quantitative) behavior for any location of the atoms. Likewise, we wanted easy constraint of parameters derivable from other sources (e.g., vibrational frequencies and dissociation energies of the diatomics), and easy adjustability of parameters that can be approximately determined by comparison to the experimental data (e.g., barrier heights, complex well depth or vibrational frequencies).

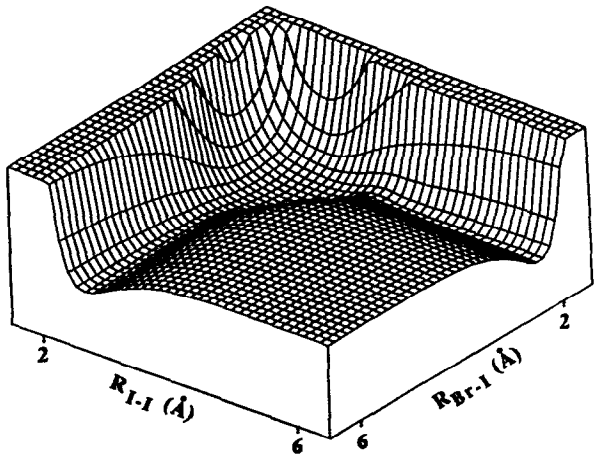

FIG. 11. Three-dimensional view of the reactive PES at a bond angle of 150°.

Table I summarizes the various coefficients in the PES formula (see the Appendix), with a brief description of the physical meaning of each. In the present calculations, it was also necessary to introduce an exit channel barrier to reproduce the observed long lifetimes (see the Appendix for further details), and its parameters are also listed at the end of the table.

Figure 11 shows a 3D plot of the optimal PES for $\theta=150°$; Fig. 12 shows the PES at four different values of θ_3 (corresponding to a BrII rather than an IBrI complex), with the parameters given in Table I; this corresponds to one of the "best fit" potentials discussed in the next section, with a significant well, an exit channel barrier, allowing only a small amount of interconversion near the reaction threshold to a less strongly bound IBrI conformer, and an equilibrium bond angle fixed near 150°.

D. Dynamics

A number of workers have reported classical trajectory calculations on trihalogen complexes. Thompson has performed Monte Carlo trajectory calculations for $X+X_2$ (X =Cl,Br, and I) on surfaces based on the London or LEPS formalism.[103] In all three cases, the PESs contain shallow wells, and produce at least some long-lived trajectories indicative of a collision complex. Collisions of F with heavier halogens have been extensively discussed in the literature. The surface used by Fletcher and Whitehead contains a very shallow well, but they nonetheless find a symmetrical scattering distribution indicative of the formation of collision complexes.[107] Urrecha *et al.*[109] have studied the dynamics of the F+ICl reaction on surfaces with a late, deep well (31 kcal mol^{-1} with respect to reactants for attack on the I atom) and find lifetimes of up to 6 ps. This results in a number of vibrational periods of the complex comparable to what is found in the present study, due to the smaller reduced mass and stronger bond in the FICl complex

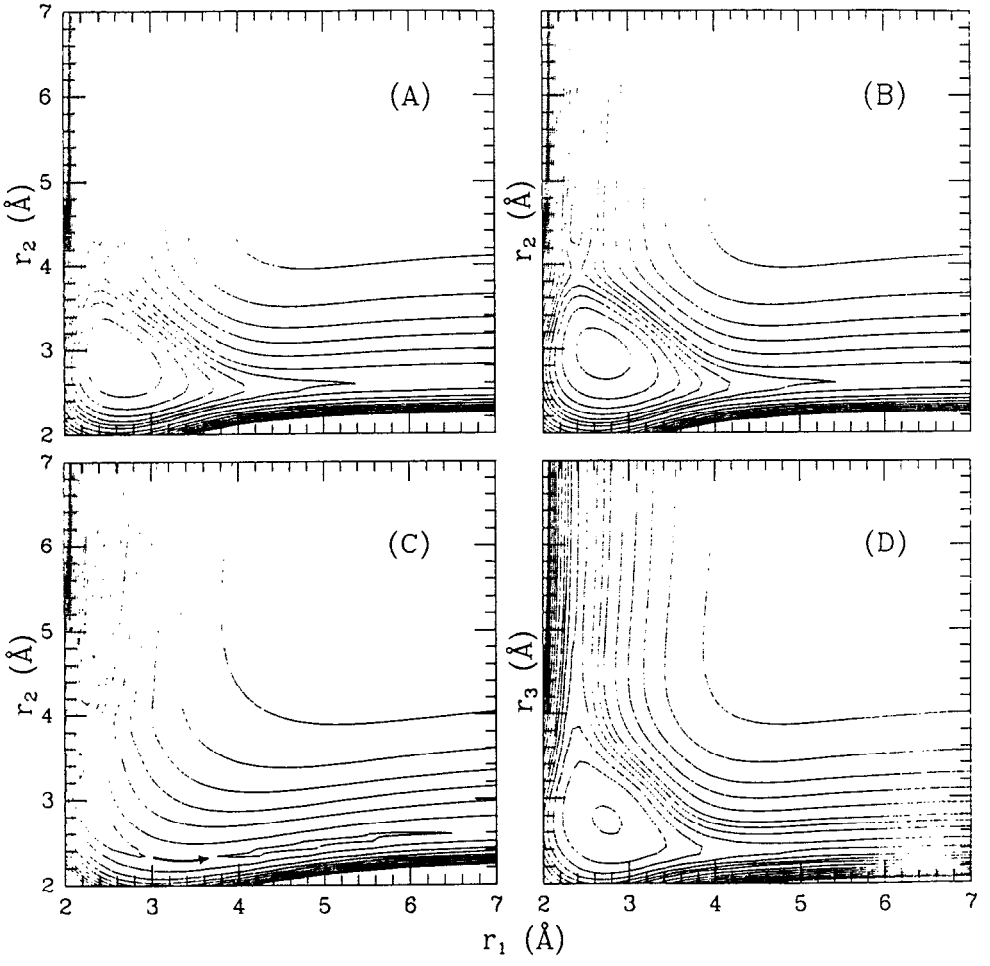

FIG. 12. Cuts through the PES. (A) shows r_1 (r_{Br-I}) vs r_2 (r_{I-I}) at 180°; (B) shows the lowering of the potential energy as the molecule is bent to 150°; (C) shows are very strongly bent 60° configuration, where the arrow indicates a transition from an IBrI to a BrII complex for a sufficiently energetic trihalogen molecule; (D) is a projection onto r_1–r_3 space, showing the symmetric dissociation limits of the IBrI complex.

model than in the BrI_2 case. Finally, Borne and Bunker have reported three-dimensional calculations on $Br+I_2$ on a variety of "early" and late surfaces.[110] They concluded that a potential well of 5–10 kcal mol^{-1} does not strongly affect the scattering angles, indicating the absence of long-lived complexes. This is in contrast to a later study by Fitz and Brumer, which shows that, as in the case of other trihalogen complexes, inclusion of a well in the PES results in the formation of collision complexes.[110]

In the present case, integration of Hamilton's equations of motion was carried out in space-fixed or triatomic center-of-mass coordinates, using a Bulirsch–Stoer routine with adaptive stepsize supported by an adaptive fourth order Runge–Kutta method near singular points.[111] The stepsize was typically on the order of 0.5 to 5 fs, with an accuracy of at least one part in 10^7 per step. Trajectories were tested in a number of ways: Energy conservation was enforced for all trajectories to 5 parts in 10^6 between beginning and end points. It was found that even at the maximum precision ($1:10^9$) of the integration procedure, trajectories could not be backintegrated reliably after more than 10 ps, where the accumulated deviation amounted to $\approx$0.02 Å. This is due to the chaotic nature of the trajectories, and because of ergodicity does not effect *averaged* quantities (e.g., lifetimes) even at t larger than 10 ps.[112]

We now consider the results for reactions starting from the van der Waals impacted geometry, followed by calculations simulating crossed-beam scattering experiments.

1. Reactions from van der Waals impacted geometries

For the van der Waals precursor calculations, the following Monte Carlo selected initial conditions were used: The I_2 molecule was held in $v=0$, with a random vibrational phase and zero space fixed angular momentum. The Br atom was placed near collinearly at 5.47 ± 0.1 Å from the I_2 center of mass with a small Gaussian spread in the plane normal to the I–I bond, corresponding to the nonaxial intramolecular vibrations in the van der Waals precursor. The Br was given an initial velocity of 2.4 ± 0.1 Å/ps (HBr precursor) or 3.4 ± 0.1 Å/ps (DBr precursor) in the space-fixed frame. It was mentioned earlier that the equilibrium geometry of the complex is particularly uncertain as regards the distribution of hydrogen orientations.

TABLE II. Representative calculated complex lifetimes in ps under various conditions, including number of bonds (# bonds, 2 is collinear, 3 is a full calculation with three vibrational and three rotational degrees of freedom), well depth (Well, in kcal mol^{-1}), exit channel barrier height (Barrier, in kcal/mol^{-1}), average hydrogen/deuterium bending angle for van der Waals precursor reactions (Angle, degrees), van der Waals precursor or crossed beam calculation (vdW/CB), and translational energy of the Br atom (E_T in cm^{-1}, not including van der Waals interaction energy). The asterisks mark the optimal surface parameters used in the text.

Lifetime	# bonds	Barrier	Well	Angle	vdW/CB	E_T
6(1)	2	0	10	0	vdW	145
6.2(5)	2	0	20	0	vdW	145
11(1)	2	4	10	0	vdW	145
3.0(5)	3	0	12.5	-	CB	980
5.3(5)	3	0	15	0	vdW	290
6.5(5)	3	0	15	0	vdW	145
3.7(5)	3	0	15	-	CB	980
7(1)	3	0	15	55	vdW	290
8(1)	3	0	15	55	vdW	145
20(4)	3	3.5	12.5	-	CB	290
27(2)	3	3.0	15	0	vdW	290
25(4)	3	2.9	15	0	vdW	290
38(4)	3	3.0	15	0	vdW	145
41(5)	3	2.7	15	55	vdW	290
52(5)	3	2.7	15	55	vdW	145
8(1)	3	2.7	15	-	CB	980
9(1)	3	3.5	15	-	CB	980
51(5)	3	3.0	15	55	vdW	290
64(6)	3	3.0	15	55	vdW	145
40(4)	3	3.4	16.2	0	vdW	145
35(4)	3	3.4	16.2	0	vdW	290
38(4)	3	3.5	17.5	0	vdW	290
58(4)	3	3.5	17.5	0	vdW	145

Two types of calculations were carried out, with the most probable initial Br velocity vector oriented either along the Br–I–I axis, or at 55° from it. The large amplitude motion of the H was accounted for by a Gaussian spread of 12.5° HWHM (for the HBr case, correspondingly smaller for the DBr case). Where appropriate, 2σ Monte Carlo uncertainties, derived by randomly binning trajectories into subsets and calculating standard deviations, are quoted.

Depending on whether the van der Waals kinetic energy was assigned randomly to the Br atom or not, trajectories ran either with an energy spread of ≈ 20 or ≈ 150 cm^{-1}. The latter has the effect of smoothing somewhat the lifetime as a function of energy, but since the lifetime is still a sufficiently slowly varying function of energy in the region of interest, and considering the uncertainties inherent in the PES itself, small differences in the sampling of initial conditions were not found to lead to quantitatively significant differences. In either case, the reaction energy is somewhat *below* the threshold value possible in a scattering experiment, resulting in a "trapped" reaction with 100% reaction probability.

Table II summarizes typical results for the complex lifetimes (HBr precursor) as a function of the dimensionality of the PES, the well depth, and the exit channel barrier height. It can be seen from the barrier-free calculations, that the addition of the bending mode increases the lifetime of the complex by about a factor of 3. However, it alone cannot account for the experimentally observed long lifetimes for any physically reasonable value of the well depth (25 kcal mol^{-1} with respect to reactants).

An exit channel barrier is required to reproduce lifetimes longer than about 10 ps, even close to the reaction threshold. Barrier heights between 2 and 4 kcal mol^{-1} (with respect to I+IBr), dependent on the depth of the well, yield the observed 50 ps lifetime for the HBr precursor reaction. There is clearly an indeterminacy, with lower

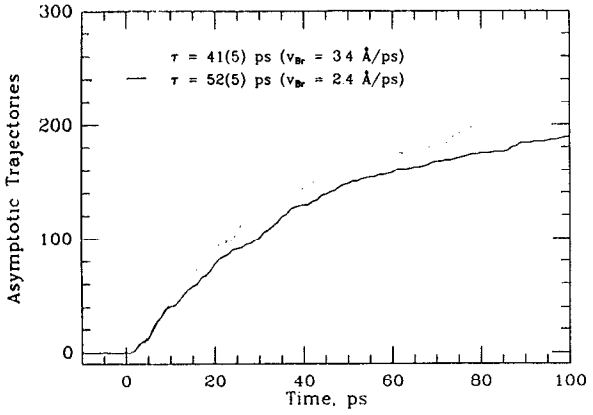

FIG. 13. Simulated transient from a best fit PES for the reaction initiated with a DBr precursor (dotted line); the same for the case of the HBr precursor (solid line), shows the increase in lifetime at slightly lower reaction energy.

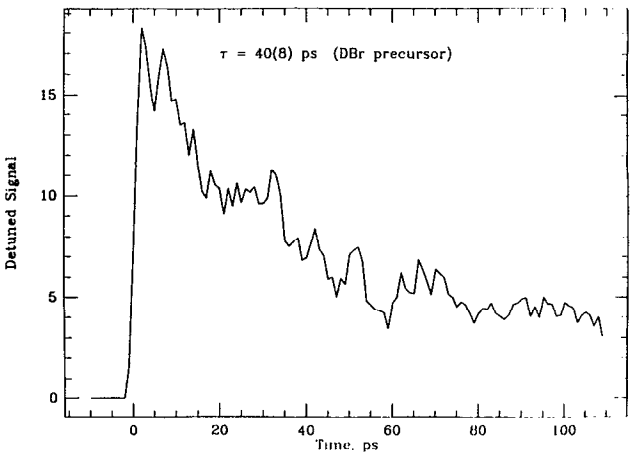

FIG. 14. Theoretical simulation of the complex decay obtained by shifting the region where trajectories can lead to detection to smaller Br–I distances in the exit channel, the case of a perturbed BrI molecule. Some of the noise is due to the Monte Carlo error in fully sampling 100 trajectories.

barriers and deeper wells yielding similar results to higher barriers and shallower wells. In the extreme case, the complex can of course be trapped for an arbitrarily long time even in a very shallow well (measured with respect to the reactants).

This indeterminacy can be removed by considering the reaction at two different energies, as provided by the HBr and DBr precursors: the calculations now have to predict not just $\tau_{av}=(\tau_{HBr}+\tau_{DBr})/2$, but also the difference, $\tau_{HBr}-\tau_{DBr}$. For a very shallow well to result in a 40 ps lifetime for the DBr case, the barrier height must be only slightly below the reaction energy. The HBr precursor trajectories would then be trapped, or at least much longer-lived than observed. On the other hand, for a very deep well and small barrier, the two precursors would result in nearly identical behavior, since an energy difference of only 145 cm^{-1} in the center of mass system, given a well of several 1000 cm^{-1} and an exothermic reaction, will have no pronounced effect on the lifetime.

This is illustrated in Table II, which shows trajectory lifetimes for HBr and DBr precursors for various well depths and barrier heights. We find that for a collinear approach geometry, a well depth of about 16 kcal mol^{-1} and a barrier height of about 3.3 kcal mol^{-1} yield the best agreement. For a 55° average approach angle, the lifetime increases by about 20% for a given set of potential parameters, and the best agreement with experiment is obtained for a well depth of about 15 kcal mol^{-1} and a barrier height of about 3.0 kcal mol^{-1}. These results are very similar to those we reported in a previous communication, using a different (r_1,r_2,θ rather than bond distance) parameterization of the PES.

Indeed, we find that the above results are relatively insensitive to the exact form of the PES used. Several trial PESs with a tighter or later complex geometry (smaller r_{el} value), different vibrational frequencies (β_{li}), and different attainment of the asymptotic limits (γ), different barriers to rearrangement (IIBr to IBrI, D_1, and D_2) resulted in less than a 30% change in the lifetime, or well depths in the range 13–17 kcal mol^{-1} and barriers in the range of 3–4 kcal mol^{-1}.

The given ranges for the barrier and well are probably indicative of the accuracy of the QCT results. It should be noted that in order to reproduce τ_{HBr}–τ_{DBr} properly, the barrier height must be adjusted to a precision of 0.1 kcal mol^{-1}. The accuracy of this value will nonetheless be considerably lower (1 kcal mol^{-1}), as the nature of the $I_2\cdots Br$ attractive potential in the 4–5 Å range determines the reaction initial energy with respect to the products. As it changes by a few hundred cm^{-1}, so must the exit channel barrier to accommodate the experimental observations (e.g., while the present observations do not allow for a fully developed barrier in the entrance channel, an incipient barrier would raise the starting energy of the trajectories).

The above calculations were done with relatively large barriers to interconversion, typically allowing only 1%–10% of trajectories to lead to the formation of the IBrI configuration. With very low barriers, the lifetime for a given exit channel barrier was lowered due to the shallower well of the symmetrical species. Should the interconversion probability be very high, the above results must be taken as averages over the available configurations, instead of reflecting the nature of a single potential well. Detailed *ab initio* calculations will be required to resolve this problem.

Figure 13 shows simulated transients for both the HBr and DBr precursor cases (conditions marked by an asterisk in Table II). They can be fitted by single exponentials, resulting in lifetimes close to those observed experimentally. The present Monte Carlo sampling is not yet accurate enough to reveal structure in the transients. The transients shown are for all vibrational levels, but since the $v=1$ population amounts to half the $v=0$ population (see below), multiexponential behavior would be evident in the transients if the lifetime were strongly vibrationally dependent.

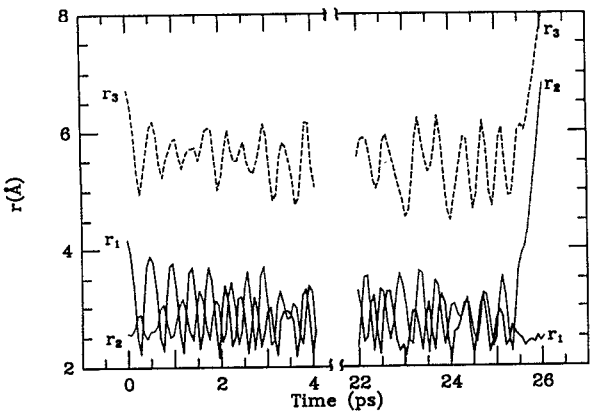

FIG. 15. The beginning and end of a typical trajectory leading to IBr product formation. The oscillations in r_3 are seen to be slower than those in r_1 and r_2, since they are more strongly correlated to the bending mode in a Br–I–I configuration.

We have also investigated the possibility of off-resonant transients probing the BrI–I complex before complete separation into products occurs. To simulate a probe window, trajectories were weighted at each point in time by a gaussian function located in the nonasymptotic range of the exit channel (near $r_{Br-I}=2.47$ Å, $r_{I-I}=3.9$ Å). The detuned transient is shown in Fig. 14. With only a fraction of the IBr molecules probed unperturbed, an "exponentially" decaying transient is observed, which levels off to a small nonzero value at long times. This falling transient resembles the statistical decay of the parent in a unimolecular process, but with a rise time limited by the complex formation time (0.5–1 ps). This "quasiunimolecular" behavior of the BrI_2 complex is to be expected, since the lifetime of the trihalogen is much longer than its "preparation" time via the reactive collision event. Otherwise, at least a biexponential would be required to fit the sequential formation and decay processes. The structure on the decay

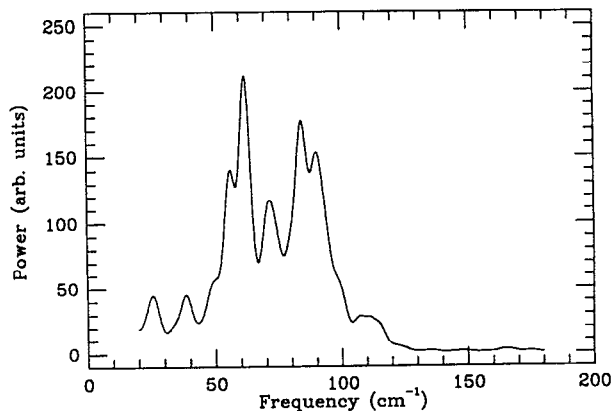

FIG. 16. The power spectrum corresponding to Fig. 15, obtained by Fourier transformation, is representative of those found for all trajectories; the period near 55 cm^{-1} corresponds to bending motion, the broader peak near 90 cm^{-1} to stretching motions of the complex.

transient falls within the 2σ Monte Carlo limits of the simulation, although the possibility of structure on the decay transients, as on the rising transients, cannot be discounted, and might be observed in experiments.

Figure 15 shows the change with time of the three bond coordinates for a typical trajectory, and Fig. 16 its power spectrum (obtained by Fourier transforming and summing the time series for the three bond coordinates), revealing a broad peak near 90 cm^{-1}. This regularity is due to the fact that the complex is still strongly bound in the symmetric stretching coordinate (by approximately the bond energy of I_2), although it is unbound in the antisymmetric normal coordinate. Due to the latter, the level density of quasibound "symmetric resonances" (estimated to be ≈ 10 cm^{-1} wide from Fig. 16) is high, which may mask the observation of an energy dependent resonance.

2. Reaction from fully impacted geometries

In addition to calculations near threshold, we have also performed QCT simulations of scattering experiments. Initial conditions were chosen in the standard way. The exact beam conditions are generally not stated in the literature, but the following should represent a reasonable approximation. The I_2 molecule was placed with its center of mass at the origin in $v=0$, with a rotational temperature of 100 K and random vibrational phases and spatial orientation. The Br atom was set to approach with a Laval-type compressed thermal distribution (average space-fixed velocity 6.4 Å/ps) of translational energies,[16] similar to the conditions reported in Ref. 14. Impact parameters were sampled with the standard radial weighting factor up to 10 Å; at larger impact parameters, the reaction probability became negligibly small. At nearly 1000 cm^{-1} above the reaction threshold, the role of the exit channel barrier in the complex lifetime drastically decreases: We found an average lifetime of 8 ps. Comparing with Table II, this is similar to the value obtained at threshold with a 15 kcal mol^{-1} well, but no exit channel barrier; At higher reaction energies, the effect of the well is thus still felt undiminished, resulting in a shorter lived complex, while the influence of the barrier has dwindled. The fact that the shorter lifetime is not due to the larger impact parameters in the scattering experiments is further supported by simulations under scattering conditions, but near threshold, which also show long lifetimes (30 ps). The smaller importance of the barrier at higher energies satisfactorily explains the (potentially) shorter lifetimes observed in the crossed-beam experiments (see below for a discussion of the crossed-beam lifetime estimates).[14]

3. The reaction at the asymptote

We have also calculated several asymptotic quantities, such as the translational energy distribution and the vibrational and rotational energy distributions. These are shown in Fig. 17 for the DBr precursor (The HBr curves are similar), with and without a 3 kcal mol^{-1} exit channel barrier and a well depth of 15 kcal mol^{-1}. The product relative translational energy distribution shows marked

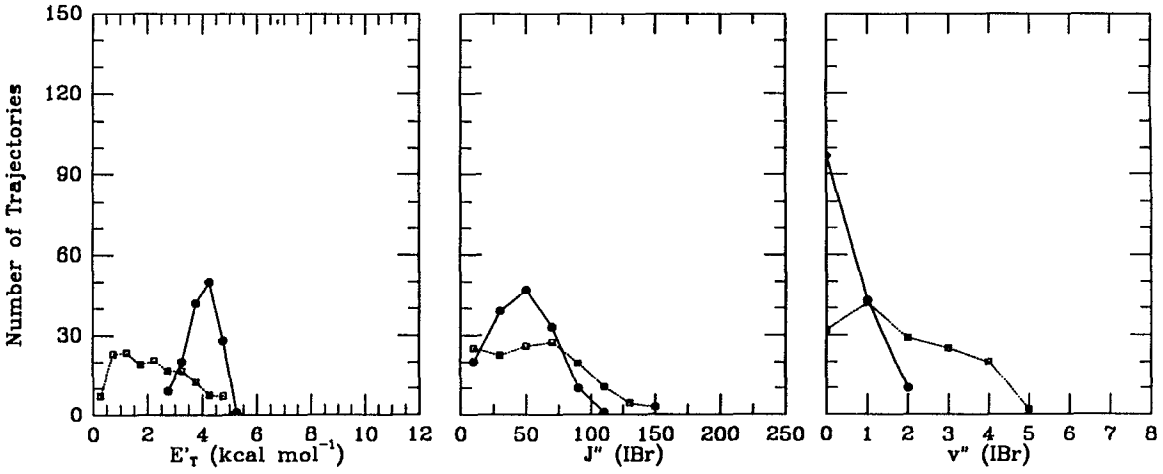

FIG. 17. Product state distributions for the DBr precursor case; the solid lines correspond to a 3 kcal mol^{-1} exit channel barrier, the dotted lines to a PES without exit channel barrier. Note that the energy stored in overall angular momentum L is not plotted, resulting in a slight energy defect if the other contributions are summed. Overall energy conservation was rigidly enforced.

threshold behavior, due to the presence of the exit channel barrier. Correspondingly, the vibrational product distribution is much colder in the barrier case ($T_{\text{eff}} \approx 380$ K for $v=0,1$, even lower for higher v states), since more energy is channeled into the translational degrees of freedom. The rotational temperature of the IBr released by the reaction is very similar, about 420 K. It would be interesting to perform experiments probing different IBr vibrational levels, to confirm the relatively cold product state distribution and the nonstatistical behavior evident in some of the distributions.

Figure 18 shows similar results for the scattering simulations. The relative I–IBr translational energy again shows "threshold" behavior in the case of an exit channel barrier, confirming tentative previous results (Fig. 19).[16] The distribution is much broader towards higher energies than in the threshold case, due to the ≈ 3 kcal mol^{-1} higher average reaction energy. As expected, the distributions are somewhat "hotter" than those calculated for the threshold case.

E. The lifetime from crossed-beam experiments

The difference between the measured near-threshold complex lifetimes presented here and higher energy (1000 cm^{-1}) estimated values based on beam experiments merits more detailed consideration. The lifetimes from scattering studies are obtained from the scattering asymmetry, with an estimated rotational period of the complex as a benchmark, as shown by Herschbach's group. To relate the lifetime to the scattering asymmetry, a simplified long-range potential and a number of other assumptions must be invoked in the analysis.

In somewhat more detail, the procedure adopted by

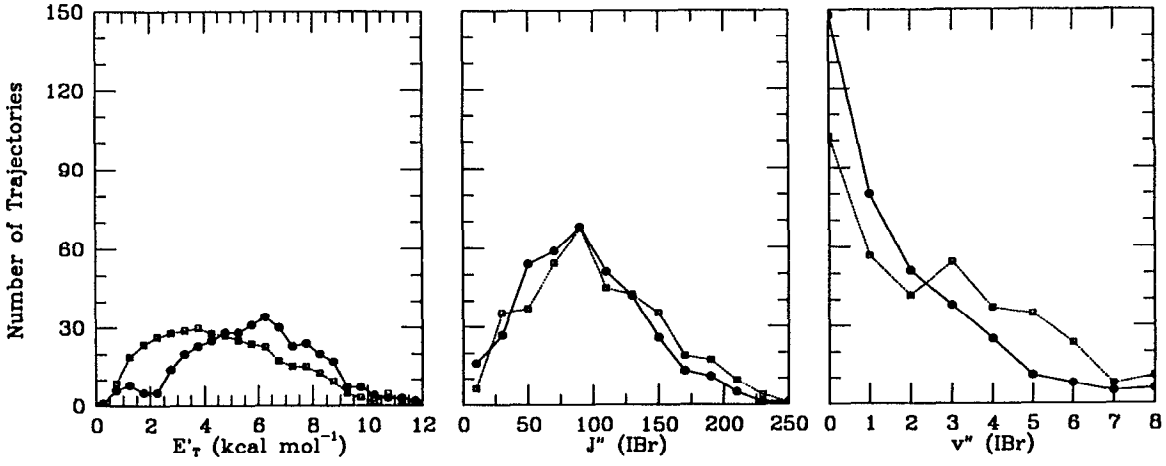

FIG. 18. Product state distribution for the crossed-beam simulation; the qualitative trend of the curves is similar to that of Fig. 17, but due to thermal averaging and the higher reaction energy, the distributions are considerably broader.

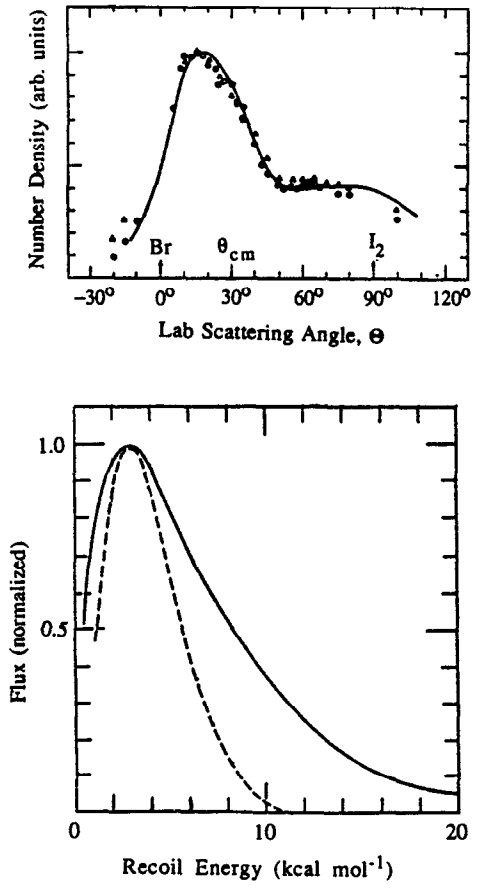

FIG. 19. Crossed-beam results for Br+I_2 ($E_T \approx 980$ cm^{-1}) taken from Ref. 16. The upper panel shows the laboratory angle scattering and translational energy distributions, the lower panel the expected translational energy release; the solid line corresponds to a nominal kinematic analysis, the dashed line to a collision-complex calculation; both show a maximum near 3 kcal mol^{-1}.

Lee *et al.*[14] and McDonald[16] can be summarized as follows. At the larger impact parameters prevalent in scattering studies, the formation of a collision complex is postulated to depend on crossing the centrifugal barrier in the long range part of the effective interaction potential,

$$V_{\text{long}}(R,L)=\frac{L^2}{2\mu R^2}-\frac{C}{R^6}. \tag{1}$$

This approximate potential has a centrifugal barrier whose height W_L depends on the angular momentum $L=mvb$ (b is the impact parameter, μ is the diatom–atom reduced mass, v the relative velocity)

$$W_L=\frac{L^3}{3\mu^{3/2}(6C)^{1/2}}. \tag{2}$$

At a given collision energy $E=\frac{1}{2}\mu v^2$, only trajectories with $E>W_L$ can clear the barrier and lead to a collision complex. There is thus a maximum value of the angular momentum (L_m) beyond which $W_L>E$ and no reaction occurs. For impact parameters b larger than $b_m=L_m/\mu v$, no collision complex is formed.

The idea is that for "long-lived" complexes, the scattering distribution $I(\theta)$ will be "forward–backward," while "short-lived" complexes should display an asymmetric scattering distribution $I'(\theta)$. The crossover occurs when the lifetime τ_{cc} is comparable to the rotational period τ_r of the complex—Herschbach's osculating complex model. In the simplest limit,[114] this can be approximated by

$$\tau_r \approx \frac{2\pi I^*}{L_m} \tag{3}$$

assuming a quasilinear complex with a moment of inertia I^*. This is only a lower limit, since $L<L_m$ for many impact parameters.

More rigorously,[16,115] the total angular momentum of the complex will be $\mathcal{J}=\mathbf{L}+\mathbf{J}$, where J is the internal angular momentum of the reactants, and usually $\mathcal{J}\approx\mathbf{L}$. If one then postulates a *nearly collinear* collision complex, which can be approximated by a prolate, nearly symmetric top, uses a Boltzmann distribution for J, and assumes a *cutoff* for $\mathcal{J}$ given by L_m, one can derive an angular distribution. As the lifetime of the collision complex becomes longer than the rotational period, it becomes very difficult to deduce it from angular distributions. In scattering experiments, if the complex is long lived, the standard method is to increase the collision energy and observe the change in angular distribution. In some reactions, however, distributions do not follow the expected long to short lifetime change.[116] Comparisons between real-time data and crossed-beam results will be useful as one examines the collision complex dynamics and asymptotic regions of the reaction.

In the case of Br+I_2, some asymmetry was observed, indicating that the complex lifetime may be comparable to or slightly larger than its averaged rotational period (see Fig. 14). This leads to a lifetime on the order of 5 ps at a calculated excess energy of ≈ 1000 cm^{-1}, since this corresponds approximately to the calculated effective rotational period of the quasilinear complex after thermal and impact parameter averaging.[14] Our QCT calculations indicate a lifetime of 8 ps under these conditions, and show that the drastic shortening of the lifetime between (sub)threshold conditions and 1000 cm^{-1} is likely due to less sensitivity to the exit channel barrier at higher energies. Nonetheless, the well at the activated complex geometry still plays an important role even at 1000 cm^{-1}, since otherwise a lifetime ≈ 3 ps would be expected. Since the crossed beam study probed the reaction in a regime where the lifetime was almost too long for a reliable estimate based on the osculating complex model outlined above, further time-resolved studies with R–Br molecules resulting in higher translational energies of the bromine atom will be required to fully reveal the dependence of complex stability on reaction energy.

V. CONCLUSIONS

We have described the real-time technique we used for the determination of collision complex lifetimes of isolated

bimolecular reactions, down to the 300 fs time scale, or better if necessary. This improved temporal resolution may well be required for the study of reactions which proceed via a shorter lived collision complex or even directly. The choice of binding partners to the precursor atom or radical opens up a wide energy range from threshold on up for direct time-resolved studies of such reactions.

The near-threshold information is sensitive to features on the PES, and allows one to study the effect of bonding (e.g., entrance or exit channel barriers, stable complex wells), on the reaction dynamics. The presence, absence, or quantitative nature of these effects can be studied, particularly if the time-domain data is combined with the wealth of available spectrally and spatially resolved experiments. As shown for the example given here, $Br+I_2$, the collision complex lifetime is directly related to the nature of the PES in the transition state region, and trajectory calculations[117] help elucidate the nature of the dynamics.

There are several improvements that we can add to a study of this type in the future. When off-resonance (complex) detection is made and the signal-to-noise ratio is improved, we may be able to resolve "structure" on the transients (steps, beats, biexponentiality, or long-tail effects). Second, extension to other families of halogens, as was made in the crossed-beam studies, would be valuable. Of particular interest is the study of light atom reactions with halogens in analogy with Polanyi's chemiluminescence, and halogen atom (or photon) + halogens, in analogy with Herschbach's, Lee's, and Wilson's studies. On the theoretical side, the calculation presented so far was classical, and future quantum calculations may indicate long-lived resonances[118,119] that have an overall effect on the lifetimes.

ACKNOWLEDGMENTS

This work was supported by a grant from the National Science Foundation. We are grateful for the very helpful discussions we have had with Professor D. Herschbach and Professor M. Okumura, and would like to thank Professor J.D. McDonald for providing additional information on the original scattering experiments done at Harvard (Ref. 16). Arthur Amos Noyes Laboratory of Chemical Physics, Contribution No. 8576.

APPENDIX

When developing the model PES for this system, the following factors were taken into account.

(1) There are three electronic states generated from the combination of a ground state atom and a ground state diatomic molecule. One state correlates to spin–orbit excited Br, which is unimportant due to symmetry considerations (see below). Another state is expected to have an entrance channel barrier and a shallow well (see Fig. 9). This leaves only one state to consider.

(2) Based on Fig. 10 one can derive a strong propensity rule, as found experimentally in Refs. 62–69 and discussed in Ref. 96: Due to the noncrossing rule for states of the same symmetry, and since Br* and I* both have $\Gamma_{1/2}$ symmetry and lie at higher energy than the $\Gamma_{3/2}$ ground state, *the reaction* $Br^* + I_2 \rightarrow BrI + I$ *is not allowed* via a bent complex, and allowed in the linear case only when a crossing of $\Gamma_{1/2}$ and $\Gamma_{3/2}$ states occurs.

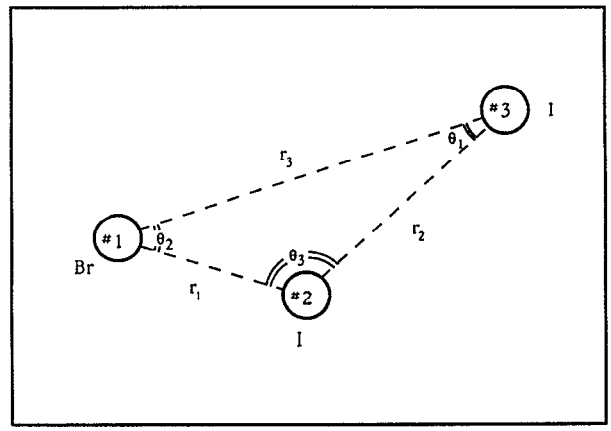

FIG. 20. The numbering of the bond coordinates, angles, and nuclei as used in the Appendix.

(3) Theoretical studies indicate that the complex should be linear or slightly bent (typically 150°) for XY_2 or X_3.[53,55,56,94] These results have been confirmed by more recent experimental reassignments of matrix-isolated ir spectra of trihalides.[48] As expected, the calculated barriers to linearity are fairly small in most cases, typically ranging from 1.5 kcal mol^{-1} (in I_3)[96] to 4 kcal mol^{-1} (in F_3),[95] and 2–6 kcal mol^{-1} (Cl_3).[90]

(4) The presence of entrance or exit channel barriers has been debated theoretically.[102,109,120] However, the results from scattering experiments and this work suggest that there is not a significant entrance channel barrier but a significant exit channel barrier is present.

(5) The complex with the less electronegative atom in the middle is expected to be more stable than alternate conformations.[98,121] Therefore, we have generally kept the interconversion barrier high enough so that the "insertion" configuration plays only a minor role.

The potential is expressed in terms of the three bond coordinates, rather than two coordinates and a bond angle, to emphasize the symmetry between the three different possible reactant combinations, complexes, and product combinations. The coordinates and numbering scheme are shown in Fig. 20. The general basis of our approach is a combination of a single global Morse potential with exponentially interpolated parameters,

$$V(r_1,r_2,r_3)=D(1-e^{-\beta x})^2-D, \tag{A1}$$

where D is the dissociation energy measured from the bottom of the well, β the vibrational parameter ($=D_e/4\omega_e x_e$ in the diatomic limit), and x a distance parameter defined by

$$x(r_1,r_2,r_3)=\frac{x_1 e^{\gamma(r_2+r_3)}+x_2 e^{\gamma(r_1+r_3)}+x_3 e^{\gamma(r_1+r_2)}}{\Sigma}, \tag{A2}$$

where Σ is the sum of the three exponential weighting factors in the numerator, and the x_i are the usual unitless

Morse distance parameter $x_i=(r_i-r_e)/r_e$. γ defines the range over which the system is not separable into an atom and a diatomic molecule.

The changes in dissociation energy, vibrational frequencies, and the local equilibrium bond distance at different bond distances can also be represented by exponential interpolation. However, in the case of D, β, and r_e, the additional ability to deviate from a smooth interpolation near the transition state is required. In general, a parameter like D, β, or r_e can be represented by $f=f_0+f_1$, where f_0 is the smoothly interpolated part

$$f_0(r_1,r_2,r_3)=\frac{f_{01}e^{\gamma(r_2+r_3)}+f_{02}e^{\gamma(r_1+r_3)}+f_{03}e^{\gamma(r_1+r_2)}}{\Sigma}, \quad \text{(A3)}$$

and f_1 becomes important only near the transition state complex. (f_{0i} are the values in the corresponding isolated diatomic molecule, e.g., D_{02} the dissociation energy between atoms 2 and 3, see Fig. 20.)

To allow for a well or saddle point near the transition state geometries, or adjust the vibrational parameters, the term f_1 must be included. There are, in general, three different equilibrium configurations (or saddle points), depending on which atom is centrally located. For a complex with equal bondlengths and a 60° equilibrium angle, a single minimum in D would be required. To break the symmetry between r_1, r_2, and r_3 at the three complex geometries with equilibrium angles of either θ_1, θ_2, or θ_3, and create three different minima, we introduce an effective equilibrium value for each bond distance,

$$\rho_i(r_j,r_k)=\sqrt{r_j^2+r_k^2-2r_jr_k\cos(\theta_{ei})}. \quad \text{(A4)}$$

f_1 is then defined as

$$f_1(r_1,r_2,r_3)=\sum_{i=1}^{3} f_{1i}e^{-[(r_j-r_e)^2+(r_k-r_e)^2]/\sigma_{f1}^2-(r_i-\rho_i)^2/\sigma_{f2}^2}, \quad \text{(A5)}$$

with cyclic permutation. The result is that, as a complex is formed, f_1 becomes nonzero. In the case of the dissociation energy, the smooth change from diatom+atom reactants to products is now interrupted by either a well ($D_{1i}>0$) or a saddle point ($D_{1i}<0$). Note that the above definition can strictly be applied only to D and β; in the case of r_e, its occurrence in the Eq. (5) must be replaced by r_{e0} or $r_{e0}+r_{e1}$, as r_e has not yet been evaluated. This, and the fact that a single value of r_e is used for all three bonds presents no problem in the present case where the equilibrium bond distances in the complex are similar ($\Delta r<0.3$ Å), and could easily be remedied in the more general case.

To allow the interconversion barriers and the bent–linear energy difference to be set independently, a term D_2 is required, which reduces the local dissociation energy for the linear configuration of the complex, effectively raising the energy difference between the linear and bent geometries,

$$D_2(r_1,r_2,r_3)=\sum_{i=1}^{3} D_{2i}e^{-[(r_j-r_e)^2+(r_k-r_e)^2]/\sigma_{D3}^2}, \quad \text{(A6)}$$

with cyclic permutation.

Physically, if the D_{2i} are chosen to be negative, but smaller than the D_{1i}, the bent–linear energy difference will be larger for a given interconversion barrier. In the surfaces we have used, both cases forbidding and allowing structural rearrangement have been considered. In all cases (see Table I), the IBrI well was made shallower than the BrII well, in accordance with the discussion presented in Sec. IV B, and the linear–bent energy difference was kept near 500 cm^{-1}.

It should be pointed out that the Morse potential formulation presented above is not satisfactory at larger atom–diatom distances, since the exponential functions decay considerably faster than the van der Waals interaction between the Br and I_2. For example, for reasonable values of the potential parameters, at an atom–diatom separation of 6 Å, the above formalism predicts a lowering of the total energy of only 2.9 cm^{-1}, whereas the $-C_{Br-I2}/r^6$ van der Waals energy amounts to -53 cm^{-1}. This has little effect on the van der Waals precursor calculation, where it only shifts the effective well depth and exit channel barrier height by a fraction of a kcal mol^{-1}, but can profoundly affect scattering calculations, which can be sensitive at large impact parameters to the location of the critical impact parameter. The latter is severely underestimated by an exponential function. This deficiency can be remedied by adding an interpolated van der Waals energy to the potential, which becomes isotropic at large distances and levels off to a constant at short distances

$$\Delta V_{vdW}(r_1,r_2,r_3)=-\frac{C}{m^6+R^6}, \quad \text{(A7)}$$

where m is a screening parameter that prevents the van der Waals correction from becoming very large at small internuclear distances. The van der Waals parameter C and the average distance R are again given by exponential interpolation,

$$C(r_1,r_2,r_3)=\frac{C_1e^{\gamma(r_2+r_3)}+C_2e^{\gamma(r_1+r_3)}+C_3e^{\gamma(r_1+r_2)}}{\Sigma},$$

$$R(r_1,r_2,r_3)=\frac{R_{1-23}e^{\gamma(r_2+r_3)}+R_{2-13}e^{\gamma(r_1+r_3)}+R_{3-12}e^{\gamma(r_1+r_2)}}{\Sigma}, \quad \text{(A8)}$$

where the R_{i-jk} are the center of mass atom–diatom separations, and the C_i are the individual atom–atom van der Waals coefficients. At short interatomic distances, for a value of $m\approx4.5$ Å, this adds a nearly constant value to the energy, which can be corrected for by slightly changing the D_i. The surfaces with or without the above correction are then in agreement to a fraction of a percent, except at distances >4 Å, where the corrected surface is a much better approximation to the real interaction potential.

The exit channel barriers can be conveniently introduced by locally lowering the dissociation energy through another term, such as a Gaussian function centered at the required barrier location. For example, an exit channel barrier (in the present case, r_1 *or* r_3 small and approxi-

mately equal to the BrI bond distance, and r_2 larger) is obtained by adding a Gaussian barrier

$$B(r_1,r_2,r_3)=B_{01}G_1(r_1,r_2,r_3)+B_{03}G_3(r_1,r_2,r_3) \quad \text{(A9a)}$$

to the local dissociation energy $D(r_1,r_2,r_3)$. The Gaussian function is defined as

$$G_i(r_1,r_2,r_3) = e^{-[(r_i-r_{Bi})^2/\sigma_{Bi}^2+(r_2-r_{B2})^2/\sigma_{B2}^2+(r_j-0.5r_{Bi}-r_{B2})^2/r_{Bi}^2]}, \quad \text{(A9b)}$$

where $i=1$ or 3 and $j=3$ or 1. Entrance channel barriers can be obtained by appropriately permuting the indices.

[1] For reviews, see, A. H. Zewail, Science **242**, 1645 (1988); M. Gruebele and A. H. Zewail, Physics Today **43**, 24 (1990); L. R. Khundkar and A. H. Zewail, Annu. Rev. Phys. Chem. **41**, 15 (1990).

[2] N. F. Scherer, L. R. Khundkar, R. B. Bernstein, and A. H. Zewail, J. Chem. Phys. **87**, 1451 (1987); N. F. Scherer, C. Sipes, R. B. Bernstein, and A. H. Zewail, *ibid.* **92**, 5239 (1990).

[3] M. Gruebele, I. R. Sims, E. D. Potter, and A. H. Zewail, J. Chem. Phys. **95**, 7763 (1991).

[4] E. D. Potter, J. L. Herek, S. Pederson, Q. Liu, and A. H. Zewail, Nature (London) **355**, 66 (1992).

[5] S. Buelow, G. Radhakrishnan, J. Catanzarite, and C. Wittig, J. Chem. Phys. **83**, 444 (1985); G. Radhakrishnan, S. Buelow, and C. Wittig, *ibid.* **84**, 727 (1986); S. Buelow, M. Noble, G. Radhakrishnan, H. Reisler, C. Wittig, and G. Hancock, J. Phys. Chem. **90**, 1015 (1986); C. Wittig, S. Sharpe, and R. A. Beaudet, Acc. Chem. Res. **21**, 341 (1988); Y. Chen, G. Hoffmann, D. Oh, and C. Wittig, Chem. Phys. Lett. **159**, 426 (1989); C. Wittig, Y. M. Engel, and R. D. Levine, *ibid.* **153**, 411 (1988); S. K. Shin, Y. Chen, D. Oh, and C. Wittig, Philos. Trans. R. Soc. London, Ser. A **332**, 361 (1990); G. Hoffmann, D. Oh, Y. Chen, Y. M. Engel, and C. Wittig, Isr. J. Chem. **30**, 115 (1990); S. K. Shin, Y. Chen, S. Nickolaisen, S. W. Sharpe, R. A. Beaudet, and C. Wittig, *Advances in Photochemistry*, edited by D. H. Volman, G. S. Hammond, and D. C. Neckers (Wiley, New York, 1991), Vol. 16, p. 249; S. K. Shim, Y. Chen, E. Böhmer, and C. Wittig, in *Dye Lasers: 25 Years*, edited by M. Stuke (Springer-Verlag, New York, 1992), p. 57.

[6] C. Jouvet and B. Soep, Chem. Phys. Lett. **96**, 426 (1983); C. Jouvet and B. Soep, J. Chem. Phys. **80**, 2229 (1984); W. H. Breckenridge, C. Jouvet Duval, and B. Soep, J. Phys. Chem. **91**, 5416 (1987); J. P. Visticot, B. Soep, and C. J. Whitham, *ibid.* **92**, 4574 (1988); C. Jouvet, M. C. Duval, B. Soep, W. H. Breckenridge, C. Whitham, and J. P. Visticot, J. Chem. Soc. Faraday Trans. 2 **85**, 1133 (1989); M.-C. Duval, B. Soep, and W. H. Breckinridge, J. Chem. Phys. **95**, 7145 (1991).

[7] S. W. Sharpe, Y. P. Zeng, C. Wittig, and R. A. Beaudet, J. Chem. Phys. **92**, 943 (1990).

[8] See, A. Jacobs, M. Wahl, R. Weller, and J. Wolfrum, Chem. Phys. Lett. **158**, 161 (1989); M. J. Frost, J. S. Salh, and I. W. M. Smith, J. Chem. Soc. Faraday Trans. **87**, 1037 (1991); for recent reviews see, J. A. Miller, R. J. Kee, and C. K. Westbrook, Annu. Rev. Phys. Chem. **41**, 345 (1990); R. E. Weston, Jr., J. Chem. Ed. **65**, 1062 (1988); G. W. Flynn, Science **246**, 1009 (1989); J. K. Rice and A. P. Baronavski, J. Chem. Phys. **94**, 1006 (1991).

[9] S. K. Shin, C. Wittig, and W. A. Goddard III, J. Phys. Chem. **95**, 8048 (1991).

[10] G. C. Schatz, M. S. Fitzcharles, and L. B. Harding, Faraday Discuss. Chem. Soc. **84**, 359 (1987); G. C. Schatz and M. S. Fitzcharles, in *Selectivity in Chemical Reactions*, edited by J. C. Whitehead (Kluwer, Dordrecht, 1988); K. Kudla and G. C. Schatz, J. Phys. Chem. **95**, 8267 (1991); K. Kudla, G. C. Schatz, and A. F. Wagner, J. Chem. Phys. **95**, 1635 (1991).

[11] D. Feller, E. S. Huyser, W. T. Borden, and E. R. Davidson, J. Am. Chem. Soc. **105**, 1459 (1983); M. Aoyagi and S. Kato, J. Chem. Phys. **88**, 6409 (1988); J. Brunning, D. W. Derbyshire, I. W. M. Smith, and M. D. Williams, J. Chem. Soc. Faraday Trans. 2 **84**, 105, (1988); J. K. Rice, Y. C. Chung, and A. P. Baronawski, Chem. Phys. Lett. **167**, 151 (1990).

[12] A. H. Zewail, Faraday Discuss. Chem. Soc. **91**, 207 (1991).

[13] *Handbook of Chemistry and Physics*, 71st ed., edited by D. R. Lide (CRC, Boca Raton, 1990).

[14] Y. T. Lee, J. D. McDonald, P. R. LeBreton, and D. R. Herschbach, J. Chem. Phys. **49**, 2447 (1968).

[15] G. A. Fisk, J. D. McDonald, and D. R. Herschbach, Faraday Discuss. Chem. Soc. **44**, 228 (1967).

[16] J. D. McDonald, Ph.D. thesis, Harvard University, 1971.

[17] H. J. Loesch and D. Beck, Ber. Bunsenges. Phys. Chem. **75**, 736 (1971).

[18] D. Beck, F. Engelke, and H. J. Loesch, Ber. Bunsenges. Phys. Chem. **72**, 1105 (1968).

[19] Y. T. Lee, P. R. LeBreton, J. D. McDonald, and D. R. Herschbach, J. Chem. Phys. **51**, 455 (1969).

[20] J. B. Cross and N. C. Blais, J. Chem. Phys. **50**, 4108 (1969).

[21] N. C. Blais and J. B. Cross, J. Chem. Phys. **52**, 3580 (1970).

[22] J. B. Cross and N. C. Blais, J. Chem. Phys. **55**, 3970 (1971).

[23] C. F. Carter, M. R. Levy, K. B. Wooodall, and R. Grice, Faraday Discuss. Chem. Soc. **55**, 381 (1973).

[24] N. C. Firth and R. Grice, Mol. Phys. **60**, 1261 (1987).

[25] N. C. Firth and R. Grice, Mol. Phys. **60**, 1273 (1987).

[26] N. C. Firth, D. J. Smith, and R. Grice, Mol. Phys. **61**, 859 (1987).

[27] N. C. Firth, N. W. Keane, D. J. Smith, and R. Grice, Faraday Discuss. Chem. Soc. **84**, 53 (1987).

[28] S. M. A. Hoffman, D. J. Smith, and R. Grice, Mol. Phys. **49**, 621 (1983).

[29] J. J. Valentini, Y. T. Lee, and D. J. Auerbach, J. Chem. Phys. **67**, 4866 (1977).

[30] T. Trickl and J. Wanner, J. Chem. Phys. **78**, 6091 (1983).

[31] B. Girard, N. Billy, G. Gouédard, and J. Vigué, Faraday Discuss. Chem. Soc. **84**, 65 (1987).

[32] B. Girard, N. Billy, G. Gouédard, and J. Vigué, Europhys. Lett. **14**, 13 (1991).

[33] J. C. Whitehead, Comp. Chem. Kinet. **24**, 357 (1983).

[34] D. L. Bunker and N. Davidson, J. Am. Chem. Soc. **80**, 5090 (1958).

[35] G. Porter, Discuss. Faraday Soc. **33**, 198 (1962).

[36] V. I. Balykin, V. S. Letokhov, V. I. Mishin, and V. A. Semchishen, Chem. Phys. **17**, 111 (1976).

[37] J. L. Tellinghuisen, A. R. Whyte, and L. F. Phillips, J. Phys. Chem. **88**, 6084 (1984).

[38] J. I. Cline and S. R. Leone, J. Phys. Chem. **95**, 2917 (1991).

[39] M. W. Sigrist, D. J. Krajnovich, F. Huisken, Z. J. Zhang, Y. T. Lee, and Y. R. Shen, Helv. Phys. Acta **53**, 289 (1980).

[40] M. Kawasaki, H. Sato, and G. Inoue, J. Phys. Chem. **93**, 7571 (1989).

[41] J. J. Valentini, M. J. Coggiola, and Y. T. Lee, J. Am. Chem. Soc. **98**, 853 (1976).

[42] M. J. Coggiola, J. J. Valentini, and Y. T. Lee, Int. J. Chem. Kinet. **8**, 605 (1976).

[43] J. J. Valentini, M. J. Coggiola, and Y. T. Lee, Faraday Discuss. Chem. Soc. **62**, 232 (1977).

[44] G. Mamantov, D. G. Vickroy, E. J. Vasini, T. Maekwa, and M. C. Moulton, Inorg. Nucl. Chem. Lett. **6**, 701 (1970).

[45] G. Mamantov, E. J. Vasini, M. C. Moulton, D. G. Vickroy, and T. Maekwa, J. Chem. Phys. **54**, 3419 (1971).

[46] M. R. Clarke, W. H. Fletcher, G. Mamantov, E. J. Vasini, and D. G. Vickroy, Inorg. Nucl. Chem. Lett. **8**, 611 (1972).

[47] E. S. Prochaska and L. Andrews, Inorg. Chem. **16**, 339 (1977).

[48] E. S. Prochaska, L. Andrews, N. R. Smyrl, and G. Mamantov, Inorg. Chem. **17**, 970 (1978).

[49] L. Y. Nelson and G. C. Pimentel, J. Chem. Phys. **47**, 3671 (1967).

[50] D. H. Boal and G. A. Ozin, J. Chem. Phys. **55**, 3598 (1971).

[51] C. A. Wight, B. S. Ault, and L. Andrews, J. Chem. Phys. **65**, 1244 (1976).

[52] M. E. Jacox, J. Phys. Chem. Ref. Data **13**, 945 (1984).

[53] S. R. Ungemach and H. F. Schaefer III, J. Am. Chem. Soc. **98**, 1658 (1976).

[54] B. R. De and A. B. Sannigrahi, Int. J. Quantum Chem. **19**, 485 (1981).

[55] A. B. Sannigrahi and S. D. Peyerimhoff, Chem. Phys. Lett. **114**, 6 (1985).

[56] V. L. Pershin and A. I. Boldyrev, J. Mol. Struct. (Theochem) **150**, 171 (1987).

[57] M. A. A. Clyne and H. W. Cruse, J. Chem. Soc. Faraday Trans. 2 **68**, 1377 (1972).

[58] E. H. Appelman and M. A. A. Clyne, J. Chem. Soc. Faraday Trans. 1 **71**, 2072 (1975).

[59] P. P. Bemand and M. A. A. Clyne, J. Chem. Soc. Faraday Trans. 2 **72**, 191 (1975).
[60] P. P. Bemand and M. A. A. Clyne, J. Chem. Soc. Faraday Trans. 2 **71**, 1132 (1975).
[61] L. W. Strattan and M. W. Kaufman, J. Chem. Phys. **66**, 4963 (1977).
[62] F. Zaraga, S. R. Leone, and C. B. Moore, Chem. Phys. Lett. **42**, 275 (1976).
[63] H. K. Haugen, E. Weitz, and S. R. Leone, Chem. Phys. Lett. **119**, 75 (1985).
[64] For a review, see, I. W. M. Smith, J. Chem. Soc. Faraday Trans. **87**, 2271 (1991); I. W. M. Smith, *Kinetics and Dynamics of Elementary Gas Reactions* (Butterworths, London, 1980).
[65] H. Hofman and S. R. Leone, Chem. Phys. Lett. **54**, 314 (1978).
[66] A. Hariri, A. B. Peterson, and C. Wittig, J. Chem. Phys. **65**, 1872 (1976).
[67] J. R. Wiesenfeld and G. L. Wolk, J. Chem. Phys. **69**, 1797 (1978).
[68] J. R. Wiesenfeld and G. L. Wolk, J. Chem. Phys. **69**, 1805 (1978).
[69] E. B. Gordon, A. I. Nadkhin, S. A. Sotnichenko, and I. A. Boriev, Chem. Phys. Lett. **86**, 209 (1982).
[70] H. Okabe, *Photochemistry of Small Molecules* (Wiley-Interscience, New York, 1978).
[71] B. J. Huebert and R. M. Martin, J. Phys. Chem. **72**, 3046 (1968).
[72] F. Magnotta, D. J. Nesbitt, and S. R. Leone, Chem. Phys. Lett. **83**, 21 (1981).
[73] Z. Xu, B. Koplitz, and C. Wittig, J. Chem. Phys. **87**, 1062 (1987).
[74] Z. Xu, B. Koplitz, and C. Wittig, J. Phys. Chem. **92**, 5518 (1988).
[75] F. A. Baiocchi, T. A. Dixon, and W. Klemperer, J. Chem. Phys. **77**, 1632 (1982).
[76] S. E. Novick, K. C. Janda, and W. Klemperer, J. Chem. Phys. **65**, 5115 (1977).
[77] L.-E. Selin, Ark. Fys. **21**, 479 (1962).
[78] W. G. Brown, Phys. Rev. **42**, 355 (1932).
[79] E. M. Weinstock, J. Mol. Spectrosc. **61**, 395 (1976).
[80] E. M. Weinstock and A. Preston, J. Mol. Spectrosc. **70**, 188 (1978).
[81] M. A. A. Clyne and I. S. McDermid, J. Chem. Soc. Faraday Trans. 2 **72**, 2252 (1976).
[82] T. A. Stephenson, W. R. Simpson, J. R. Wright, H. P. Schneider, J. W. Miller, and K. E. Schultz, J. Phys. Chem. **93**, 2310 (1989).
[83] L.-E. Selin and B. Söderborg, Ark. Fys. **21**, 515 (1962).
[84] R. S. Mulliken, J. Chem. Phys. **55**, 288 (1971), and references therein.
[85] J. Tellinghuisen, Chem. Phys. Lett. **99**, 373 (1983).
[86] R. J. Donovan, B. V. O'Grady, K. Shobatake, and A. Hiraya, Chem. Phys. Lett. **122**, 612 (1985).
[87] A. Hiraya, K. Shobatake, R. J. Donovan, and A. Hopkirk, J. Chem. Phys. **88**, 52 (1988).
[88] Z. A. Yasa and N. M. Amer, Opt. Commun. **36**, 406 (1981).
[89] N. F. Scherer, J. L. Knee, D. D. Smith, and A. H. Zewail, J. Phys. Chem. **89**, 5141 (1985); M. Rosker, M. Dantus, and A. H. Zewail, J. Chem. Phys. **89**, 6128 (1988).
[90] A. B. Sannigrahi and S. D. Peyerimhoff, Int. J. Quantum Chem. **30**, 413 (1986).
[91] E. Vasini and E. Castro, J. Mol. Struct. **22**, 415 (1974).
[92] E. Castro and E. Vasini, Int. J. Quantum Chem. **22**, 433 (1982).
[93] B. M. Deb, G. D. Mahajan, and V. S. Vasan, Pramana **9**, 93 (1977).
[94] S. Bhattacharjee, A. B. Sannigrahi and D. C. Mukherjee, Ind. J. Chem A **22**, 1001 (1983).
[95] B. R. De and A. B. Sannigrahi, Int. J. Quantum Chem. **22**, 435 (1982).
[96] A. Viste and P. Pyykkö, Int. J. Quantum Chem. **25**, 223 (1984).
[97] K. Fukui, Angew. Chem. Int. Ed. Engl. **21**, 801 (1982); R. G. Pearson, Acc. Chem. Res. **4**, 152 (1971).
[98] For a review and further references, see, D. R. Herschbach, in *The Chemical Bond*, edited by A. H. Zewail (Academic, Boston, 1992), p. 210.
[99] M. Koshi, H. Ito, and H. Matsui, Chem. Phys. Lett. **103**, 180 (1983).
[100] J. J. Duggan and R. Grice, J. Chem. Soc. Faraday Trans. 2 **80**, 795 (1984).
[101] J. J. Duggan and R. Grice, J. Chem. Soc. Faraday Trans. 2 **80**, 809 (1984); **85**, 1081 (1984).
[102] L. Dalla Riva, S. H. Lin, and H. Eyring, Anal. Asoc. Quim. Arg. **59**, 133 (1971).
[103] D. L. Thompson, J. Chem. Phys. **60**, 4557 (1974); Chem. Phys. Lett. **55**, 424 (1978).
[104] J. C. Polanyi, Angew. Chem. Int. Ed. Engl. **26**, 952 (1987).
[105] N. C. Blais and D. L. Bunker, J. Chem. Phys. **37**, 2713 (1962); L. M. Raff and M. Karplus, *ibid.* **44**, 1212 (1966).
[106] D. L. Bunker and N. C. Blais, J. Chem. Phys. **41**, 2377 (1964); D. L. Bunker and C. A. Parr, *ibid.* **52**, 5700 (1970).
[107] I. W. Fletcher and J. C. Whitehead, J. Chem. Soc. Faraday Trans. 2 **78**, 1165 (1982).
[108] M. Gruebele, G. Roberts, and A. H. Zewail, Philos. Trans. R. Soc. London, Ser. A **332**, 223 (1990).
[109] I. Urrecha, I. Serna, and J. Iturbe, Chem. Phys. **154**, 85 (1991).
[110] T. B. Borne and D. L. Bunker, J. Chem. Phys. **55**, 4861 (1971); D. E. Fitz and P. Brumer, *ibid.* **69**, 1792 (1978).
[111] W. H. Press, B. P. Flannery, S. A. Teukolsky, and W. T. Vetterling, *Numerical Recipes* (Cambridge University, Cambridge, 1986).
[112] This deviation is not due to any deficiency in the routine, but rather to the presence of chaos. This was tested for by a method similar to that proposed in Ref. 113, by noting the exponential divergence of trajectories nearby in phase space and on the same energy shell (Lyapunov coefficient $\sim 3\ ps^{-1}$). The round-off error in the differential equation solver "seeds" this orbit divergence, but since the motion is ergodic, average quantities are still correct as long as energy conservation is rigorously enforced.
[113] G. Benettin and J. M. Strelcyn, Phys. Rev. A **17**, 773 (1978).
[114] M. M. Oprysko, F. J. Aoiz, M. A. McMahan, and R. B. Bernstein, J. Chem. Phys. **78**, 3816 (1983).
[115] D. O. Ham and J. L. Kinsey, J. Chem. Phys. **53**, 285 (1970); W. B. Miller, S. A. Safron, and D. R. Herschbach, *ibid.* **56**, 3580 (1972).
[116] See, for example, L. Bañares and A. G. Ureña, J. Chem. Phys. **93**, 6473 (1990); L. Bañares, A. G. Ureña, and A. A.-Navarro, J. Chem. Soc. Faraday Trans. **86**, 2063 (1990).
[117] See, J. C. Polanyi, in *The Chemical Bond: Structure and Dynamics*, edited by A. H. Zewail (Academic, Boston, 1992).
[118] G. Schatz and J. Dyck, Chem. Phys. Lett. **188**, 11 (1992).
[119] See, for example, J. D. Kress, R. B. Walker, and E. F. Hayes, J. Chem. Phys. **93**, 8085 (1990).
[120] I. Urrecha, F. Castano, and J. Iturbe, J. Chem. Soc. Faraday Trans. 2 **82**, 1077 (1986).
[121] B. M. Gimarc, *Molecular Structure and Bonding* (Academic, Orlando, 1979).